Resolving the size of ice-nucleating particles with a balloon deployable aerosol sampler: the SHARK

Grace C. E. Porter[1,2], Sebastien N. F. Sikora[1], Michael P. Adams[1], Ulrike Proske[1,3], Alexander D. Harrison[1], Mark D. Tarn[1,2], Ian M. Brooks[1] & Benjamin J. Murray[1]

[1]School of Earth and Environment, University of Leeds, Leeds LS2 9JT, UK
[2]School of Physics and Astronomy, University of Leeds, Leeds LS2 9JT, UK
[3]Institute for Atmospheric and Environmental Sciences, Goethe University Frankfurt, Frankfurt am Main, Germany

Correspondence to: Grace C. E. Porter (ed11gcep@gmail.com) and Benjamin J. Murray (b.j.murray@leeds.ac.uk)

Abstract. Ice-nucleating particles (INPs) affect cloud development, lifetime and radiative properties, hence it is important to know the abundance of INPs throughout the atmosphere. A critical factor in determining the lifetime and transport of INPs is their size, however very little size-resolved atmospheric INP concentration information exists. Here we present the development and application of a radio-controlled payload capable of collecting size-resolved aerosol from a tethered balloon for the primary purpose of offline INP analysis. This payload, known as the SHARK (Selective Height Aerosol Research Kit), consists of two complementary cascade impactors for aerosol size-segregation from 0.25 to 10 μm, with an after-filter and top stage to collect particles below and above this range at flow rates up to 100 L min^{-1}. The SHARK also contains an optical particle counter to quantify aerosol size distribution between 0.38 and 10 μm, and a radiosonde for the measurement of temperature, pressure, GPS altitude, and relative humidity. This is all housed within a weatherproof box, can be run from batteries for up to 11 h and has a total weight of 9 kg. The radio control and live data link with the radiosonde allow the user to start and stop sampling depending on meteorological conditions and height, which can, for example, allow the user to avoid sampling in very humid or cloudy air, even when the SHARK is out of sight. While the collected aerosol could, in principle, be studied with an array of analytical techniques, this study demonstrates that the collected aerosol can be analysed with an off-line droplet freezing instrument to determine size-resolved INP concentrations, activated fractions and active site densities, producing similar results to those obtained using a standard PM$_{10}$ aerosol sampler when summed over the appropriate size range. Test data, where the SHARK was sampling near ground level or suspended from a tethered balloon at 20 m altitude, is presented from four contrasting locations having very different size resolved INP spectra: Hyytiälä (Southern Finland), Leeds (Northern England), Longyearbyen (Svalbard), and Cardington (Southern England).

1   Introduction

Atmospheric ice-nucleating particles (INPs) are not well understood, with knowledge of their concentration, sources, temporal variability, transport and size in its infancy (Kanji et al., 2017; Murray et al., 2012). This is of importance because clouds between 0 °C and around −35 °C can exist in a supercooled liquid, mixed-phase (ice and water) or glaciated (ice only) state depending in part on the presence or absence of INPs (Kanitz et al., 2011; Vergara-Temprado et al., 2018). In the absence of INP, cloud droplets can supercool to below ∼−35°C (Herbert et al., 2015), but INP can trigger freezing at much higher temperatures (Kanji et al., 2017). These particles usually

38 have concentrations that are orders of magnitude smaller than cloud condensation nuclei (CCN), and have a
39 disproportionate impact on clouds because the nucleated ice crystals grow rapidly and precipitate out (Lohmann,
40 2017; Murray, 2017). In a shallow cloud, heterogeneous ice nucleation can result in dramatic reductions in cloud
41 albedo by removal of supercooled liquid water (Storelvmo, 2017; Vergara-Temprado et al., 2018), whereas in
42 deep convective clouds it can influence a web of microphysical processes in a complex way (Deng et al., 2018;
43 Kanji et al., 2017; Rosenfeld et al., 2011). Hence, a greater understanding of INP lifetime, transport and
44 distribution in the vertical profile is needed in order to better understand and model cloud processes and their
45 response to a changing climate.
46
47 The size of an aerosol particle significantly affects its lifetime and therefore transport in the atmosphere, with
48 particles of a few hundred nanometres potentially having a lifetime of weeks, whereas particles of 10 μm have a
49 lifetime of only hours (Jaenicke, 2007). While composition is recognised to be an important controller of ice
50 nucleation ability (Kanji et al., 2017), it has also been generally thought that the larger an aerosol particle, the
51 more likely it is to serve as an INP (Pruppacher and Klett, 1997). However, the lifetime of coarse mode aerosol
52 particles decreases rapidly with increasing size. Consistent with larger particles being better ice nucleators,
53 parameterisations of INPs in the atmosphere have been proposed wherein the INP concentration is related to the
54 concentration of aerosol particles larger than 0.5 μm (DeMott et al., 2010, 2015; Tobo et al., 2013). However,
55 most atmospheric measurements of INPs report the sum of INPs below some threshold size set by an inlet or size
56 cut, specified by the aerosol sampler used. For instance, DeMott et al. (2017) provides a comparison between a
57 selection of instruments for the collection and subsequent INP analysis of aerosol, where the aerosol samplers
58 have either a defined size cut-off or have collection efficiencies that decrease in magnitude above a defined size.
59 Nevertheless, there are examples of field studies in which INPs have been size-resolved (Berezinski et al., 1988;
60 Creamean et al., 2018b; Huffman et al., 2013; Mason et al., 2016; Reicher et al., 2018; Santachiara et al., 2010;
61 Si et al., 2018; Welti et al., 2009). These studies generally show that while the fine mode aerosol particles are
62 more abundant, coarse mode aerosol particles often contribute more to the INP population. In addition, the
63 activated fraction (n_n) of coarse mode aerosol is usually greater than fine mode aerosol. However, in some field
64 studies (Mason et al., 2016; Si et al., 2018), fine aerosol sometimes contributes more to the INP population than
65 the coarse mode. Therefore, there is a need to determine INP sizes when quantifying atmospheric INP
66 concentrations, as size is important for transport and lifetime and is therefore required to accurately model global
67 INP populations.
68
69 Measurements of INPs in and above the boundary layer are crucial to understanding the contribution of local
70 sources to the ice-nucleating activity in clouds, compared to transported aerosol. Aircraft measurements (e.g. Price
71 et al., 2018; Rogers et al., 2001) and mountaintop observatories (e.g. Conen et al., 2015) have been used to quantify
72 INP populations above the boundary layer. For example, it has been shown that there are differences in the INP
73 concentrations measured when in and out of the boundary layer at the High Altitude Research Station Jungfraujoch
74 (Switzerland) (Conen et al., 2015; Lacher et al., 2018). While these measurements are undoubtedly useful,
75 mountaintop measurements are only possible in locations with sufficiently tall yet accessible mountains, and
76 aircraft sampling is expensive and not necessarily possible in remote regions. It is therefore essential that
77 instrumentation is available that can be used to sample aerosol at selected altitudes (including ground level) in

78   order to determine INP concentrations throughout the vertical profile. Unmanned aerial vehicles (UAVs) are
79   becoming more widely used in atmospheric science; these allow the collection of aerosol at altitude at significantly
80   lower cost than with manned aircraft, but are limited by relatively short battery lives, usually under 1 h, and
81   potential propeller interference (Jacob et al., 2018; Villa et al., 2016).

82

83   Tethered kite and balloon systems have historically been used to make atmospheric measurements and collect
84   aerosol samples with much longer sampling times (many hours are readily achievable) at altitudes up to 2 km and
85   5 km for tethered balloons and kites respectively (Armstrong et al., 1981; Balsley et al., 1998). An advantage of
86   a balloon or kite system is that an instrument can be held at a chosen altitude for many hours without the balloon
87   interfering with measurements, as the instrument can be suspended on a line many meters below the balloon. They
88   can also stay inflated and in use for periods of many weeks, making them ideal for longer campaigns in remote
89   environments. A new instrument called the Honing On VERtical Cloud and Aerosol properTies (HOVERCAT)
90   (Creamean et al., 2018a) provides the capability to sample aerosol for subsequent INP analysis on a tethered
91   balloon or UAV, allowing both variable altitudes and static collection of non-size resolved aerosol smaller than
92   10 μm at 1.2 L min^{-1}. In the past, aerosols have been size-segregated using cascade impactors on a tethered balloon
93   system (Hara et al., 2013; Reagan et al., 1984), but balloon-borne cascade impactor systems have not yet been
94   adapted for the purpose of size-resolved INP analysis. The downsides of balloon-based platforms include the need
95   for wind speeds below around 64.4 km h^{-1} to avoid damage to the balloon, and the possibility of 'icing' of the
96   balloon and lines when deployed in a cold and humid environment, which could add to the weight of the payload
97   and cause the system to sink, or fall slowly. Nevertheless, balloon and kite-borne measurements remain a valuable
98   way to obtain continuous, high resolution measurements over a period of many hours in a single location at a
99   range of altitudes.

100

101   In this paper, the design, testing and operation of a payload named the Selective Height Aerosol Research Kit
102   (SHARK) is presented. It consists of two separate cascade impactor systems, operating at 9 and 100 L min^{-1}, for
103   the size-sorting of ambient aerosol particles from 0.25 to 10 μm, with an after-filter and top stage to collect
104   particles below and above this range for offline INP (or other) analysis. The SHARK also features an optical
105   particle counter (OPC) and a radiosonde, which provides real-time measurements of relative humidity (RH),
106   temperature, Global Positioning System (GPS) altitude and pressure. Weighing 9 kg, the payload is suitable for
107   use with a 21 m^3 or larger tethered balloon such as in Figure 1 a where the SHARK is shown in-flight. The use of
108   a tethered balloon and a high-capacity battery allow aerosol to be collected for up to 11 h at a user-selected altitude.

109   **2   The design and development of the SHARK**

110   **2.1   Instrument description**

111   The SHARK, shown in Figure 1, comprises two cascade impactors and corresponding pumps, alongside an OPC
112   (OPC-N2, Alphasense, UK) and radiosonde (S1H2-R, Windsond, Sweden), all mounted within a weatherproof
113   enclosure with a tail fin to orient it into the wind. A photograph of the internal components of the SHARK are
114   shown in Figure 1b. The two cascade impactors were employed to collect particles across different size bins:
115   Impactor 1 from 0.25-2.5 μm and Impactor 2 from 1-10 μm. Impactor 1 is a cascade impactor (U.S. Patent No.

116   6,786,105, Sioutas, SKC, UK), which requires a flow rate of 9 L min^{-1} and operates with a portable pump (Leland

117   Legacy, SKC, UK). Impactor 2 is also a cascade impactor (MSP Model 128, TSI, USA), which requires a flow

118   rate of 100 L min^{-1} at a pressure drop of 0.6 kPa (Marple et al., 1991; Misra et al., 2002), and for which a radial

119   flow impeller (Radial Blower U51, Micronel, UK) was used in reverse as a lightweight pump (~120 g). These

120   pumps maintain the volumetric flow rate through the impactors as temperature and atmospheric pressure change

121   with altitude. The pump for Impactor 1 was calibrated to apply this adjustment to at least 2.3 km (Leland Legacy

122   Sample Pump: Operating Instructions, SKC), although the presence of the after-filter may reduce the battery life

123   at this altitude. The pump for Impactor 2 is supplied by a larger battery and should be able to maintain flow to at

124   least the same altitude as the Impactor 1 pump, and over a longer period of time. The SHARK records the volume

125   of air sampled through Impactor 1 during the flight, and so if the pump battery was depleted, or the pressure drop

126   became too great before Impactor 2 had finished sampling, the Impactor 1 pump would shut down and store the

127   recorded value for later analysis. Further testing of the SHARK would be required to define a maximum altitude

128   limit that each SHARK component could operate at. In order to provide RH, temperature, GPS altitude and

129   pressure data in real-time, the sensors and transmitter from a radiosonde were integrated into the system. The OPC

130   measured aerosol size distributions, which were saved in the on-board memory. Servo-controlled caps covered

131   the sample inlets and outlets to reduce contamination during ascent and descent, as well as to protect the

132   components from cloud water. The operation of the SHARK components was controlled remotely via a radio link

133   using an Arduino microcontroller board (16 km range); once the SHARK was at the desired altitude according to

134   the constantly transmitting radiosonde, the inlet caps opened 10 s prior to the pumps and OPC starting in order to

135   initiate aerosol sampling and monitoring. The payload components, including the servo inlet covers and Arduino

136   control boards, were powered by a 5000 mAh battery (4S 14.8 V LiPo, Overlander, UK). The components were

137   assembled into the SHARK payload with the static (i.e. no wind) weight budget of 10 kg for a 21 m^3 balloon

138   (Skyhook Helikite, Allsopp Helikites Ltd., UK) in mind, hence the SHARK weighs 9 kg when fully instrumented.

139

140   The cascade impactors allow for the collection of size-segregated aerosol (further details are provided in Section

141   2.2) onto thin films (0.25 mm thickness) for subsequent off-line analysis, which can be used alongside information

142   about the aerosol size distributions obtained via the OPC and atmospheric conditions from the radiosonde. Our

143   initial focus concerns the analysis of the ice-nucleating properties of the collected aerosol, but an array of

144   analytical techniques could be applied to characterise the size-selected aerosol, including mass spectrometry,

145   DNA analysis, scanning electron microscopy (SEM) and transmission electron microscopy (TEM) (Ault and

146   Axson, 2017; Garcia et al., 2012; Huffman et al., 2013; Laskin et al., 2018).

147   **2.2   Size-segregated collection of aerosol**

148   Two separate cascade impactors were installed, each operating over different size ranges. This enabled size-

149   resolved aerosol sampling onto substrates across both the fine and coarse modes at high flow rates, while keeping

150   power consumption low enough to be run from batteries. Single impactor systems designed to operate across the

151   accumulation and coarse modes simultaneously require a relatively large pressure drop that would typically

152   require a prohibitively large (and heavy) pump and battery for this application.

153

154 Impactor 1 sorts aerosol into five size categories: <0.25 μm (this size bin is defined by the impactor after-filter
155 and is hereafter referred to as 1*a*), 0.25-0.5 μm (from stage 1*b*), 0.5-1.0 μm (from stage 1*c*), 1.0-2.5 μm (from
156 stage 1*d*), and >2.5 μm (from stage 1*e*). The size categories *b* to *e* correspond to the impactor stages where the 50
157 % collection cut-off diameter (d50) is the lower bound of each bin. The size bins and collection efficiencies for
158 each impactor were digitised from data provided by the manufacturers, (Misra et al., 2002; Product Information
159 Sheet - MSP) and are shown in Figure 2. Several collection substrates were tested by Misra et al. (2002), and the
160 dataset from the Teflon substrates was chosen to represent Impactor 1 here as that substrate most closely resembled
161 those used in this study. For Impactor 1, the particles were collected on 25 mm diameter filters of pore size 0.05
162 μm (Nuclepore Track-Etched Membrane polycarbonate filters, Whatman, UK). Filters were used as impactor
163 substrates rather than films since they have very low background contamination and are easier to obtain. Size
164 category 1*a* corresponds to an after-filter situated after Impactor 1, which comprised a 47 mm diameter
165 polycarbonate filter with a pore size of 5 μm (Nuclepore Track-Etched Membrane) to maintain the flow rate. The
166 collection efficiency of the after-filter was estimated to be 50-100 % at 0.25 μm and below (Soo et al., 2016).
167 Impactor 2 collected aerosol particles into three size categories: 1.0-2.5 μm (2*d*), 2.5-10 μm (2*e*), and >10 μm
168 (2*f*), also illustrated in Figure 2. 75 mm diameter filters of pore size 0.05 μm (Nuclepore Track-Etched Membrane
169 polycarbonate filters) were used in Impactor 2. An after-filter could not be used with this impactor since its
170 inclusion increased the required pressure drop to beyond what the pump could supply at 100 L min^{-1}.

172 A further benefit of using these two impactors in tandem is that, in the size ranges where they overlap of 1.0-2.5
173 μm (stage *d*) and 2.5-10 μm (stage *e*), the impaction efficiencies are very similar, allowing a direct comparison
174 between the two impactors in this size range. The stages are labelled *a* through *f* for the smallest to largest impactor
175 stage sizes (including the after-filter), such that 1*d* and 2*d* refer to stage *d* (1.0-2.5 μm) on Impactors 1 and 2,
176 respectively (see Figure 2). Background runs were produced by placing the substrates in the SHARK as if setting
177 up to sample, before removing and analysing them as normal to determine the contamination introduced through
178 the installation and recovery of the substrates.

180 Particle bounce, the bouncing of particles off the impaction substrate and the collection of these particles on the
181 lower stages, has previously been identified as a factor that can cause biases when aerosol is collected by cascade
182 impactors (Cheng and Yeh, 1979; Dzubay et al., 1976). The collection efficiency curves shown in Figure 2 for
183 Impactor 1 already account for some degree of particle bounce, having been determined experimentally by Misra
184 et al., (2002) using monodispersed polymer particles on a variety of substrates. However, the efficiency curves
185 for Impactor 2 are based on theoretical predictions (Rader and Marple, 1985) and so do not account for any bounce
186 effects. Since two of the stages of Impactors 1 and 2 overlap (stages *d* and *e*), it is possible to comment on the
187 possible effects, or lack thereof, of particle bounce, based on the results obtained using each of the comparable
188 stages. This is briefly addressed in section 3.4 where we show good agreement between these two impactors.

189 **2.3   Size distribution measurements**

190 The OPC produced binned particle size distributions from 0.38-17 μm every 1.38 s at a typical flow rate of 1.2 L
191 min^{-1}. The OPC was remotely operated through the use of its serial link via an Arduino microcontroller board.
192 Particle size, surface area and mass concentration data were produced from the raw OPC data, and these then used

193   to calculate the fraction of the aerosol that act as an INP (activated fraction, $n_\mathrm{n}(T)$), and to weight the INP data to

194   particle surface area , generating the ice-active site density per surface area ($n_\mathrm{s}(T)$) of aerosol. The particle density

195   used was 1.65 g cm^{-3}, as assumed by the OPC software, and they were assumed to be spherical. No correction

196   was made for the hygroscopic growth of aerosol particles as this required assumptions about the chemical nature

197   of the particles, and hygroscopic growth effects were minimised by avoiding sampling when the RH was above

198   about 80 % (see next section).

2.4   Radiosonde data

200   Utilising the radio control built into the payload, real-time data informed decisions of when to turn the pumps on

201   and off to sample. Continuous monitoring of the radiosonde data allows the user to avoid sampling under

202   conditions where RH approached 100 %, at which point aerosol particles become excessively swollen with water

203   or activated to cloud droplets. Hence, the influence of hygroscopic growth or cloud droplets on the collected

204   aerosol could be minimised. The temperature and pressure measurements allowed the volume of air sampled by

205   the impactors and OPC to be corrected to standard conditions (1 atm at 0 °C).

2.5   Housing and instrument orientation

207   The weatherproof housing consisted of an acrylonitrile butadiene styrene (ABS) polymer box with dimensions of

208   560 mm x 380 mm x 180 mm (IP67, Fibox). Holes to mount the impactors and OPCs were drilled so that Impactor

209   2 sat vertically upright and Impactor 1 was oriented 180° to Impactor 2 so that it faced downwards, ensuring that

210   both impactors were always oriented 90° to the wind. The OPC was at 90° to both impactors and facing towards

211   the front of the box, into the wind (see Figure 3a-c) See section 2.6 for the rationale of the positioning of the OPC

212   and impactor inlets. The tail fin, which is mounted to the lid of the box, was designed to keep the SHARK

213   orientated into the wind, and was fabricated from rigid polyvinyl chloride (PVC) sheet. Impactor 1 had its own

214   mounting screws by which it was attached to the box, whilst for Impactor 2 a custom mount was built. Securing

215   ropes were threaded through reinforced holes in the box and connected via a carabiner for quick and easy

216   attachment to the balloon instrument line, as seen in Figure 1a. Modular foam was used to keep all components

217   in place during flight.

2.6   Inlet sampling efficiencies via particle loss modelling

219   Calculation of the particle losses associated with the instrument inlets due to excessive wind speeds in various

220   configurations were used to inform the design of the SHARK and to minimise sampling biases in higher wind

221   conditions. The calculations were done using an open source particle loss calculator program in Igor Pro, the

222   details and assumptions for which are presented in Von Der Weiden et al., (2009). The particle loss characteristics

223   of the impactor and OPC inlets at their required flow rates were calculated for a wind speed of 0 and 24 km h^{-1},

224   the latter used as a maximum representative wind speed for operation. The wind speeds required for optimum

225   performance are <8 km h^{-1} for the impactors and OPC, but the system may experience higher wind speeds. Hence,

226   we use this modelling to guide our choice of positioning of the instrument relative to wind direction in order to

227   minimise sampling biases at the inlets. The modelling also allows us to better understand which impactor stages

228   (and OPC size bins) will be most affected by such biases. We make no attempt to correct the measurements for

229   sampling biases, since this correction itself would carry substantial uncertainty, but used the calculations to inform

230   us of the best configuration for the various inlets.

231

232   The inlet sampling efficiencies in the orientations chosen for the final design of the SHARK are shown in Figure

233   3. It is important to note that, due to their dissimilar inlet dimensions and operational flow rates, Impactors 1 and

234   2 are affected differently by the wind. The particle losses for the largest stages of each impactor are the most

235   affected. Stages *a* to *d* on both impactors are only minimally affected by losses. The losses are more significant

236   in stage e on both impactors, but the losses on 1e are greater than on 2*e* with a 50% cut off at around 5.5 μm and

237   a negligible sampling efficiency above about 8 μm on 1*e*. These calculations also demonstrate that the losses are

238   wind-speed dependent, but that in situations where there is significant wind, the results from Impactor 2 will be

239   less influenced by losses than Impactor 1 at sizes above 2.5 μm

240

241   The OPC suffers up to 1.6 times oversampling for 10 μm particles when sampling into 24 km h^{-1} wind, but when

242   oriented at 90° to the wind the collection efficiency of >6 μm particles approaches 0 % (see Figure 3c). Therefore,

243   the OPC has been positioned in the SHARK to be oriented into the wind to ensure data is collected for the whole

244   size range, with the caveat of a sub-isokinetic oversampling of larger particles.

3   Results and Discussion

246   The SHARK has been deployed at ground level and on a tethered balloon during development and testing at four

247   locations for the collection and monitoring of aerosol: Cardington (UK), Hyytiälä (Finland), Leeds (UK), and

248   Longyearbyen (Svalbard). Details of the sampling locations, periods, and instrumentation can be found in Table

249   S1 of the Supplementary Information (SI). In this section, we present the results for this set of four SHARK

250   deployments to illustrate the capabilities of the SHARK for quantifying ice-nucleating particle spectra as well as

251   demonstrating that the technique is consistent with more established methods.

3.1   Meteorological and aerosol size distribution data from a SHARK flight

253   An example of the radiosonde and OPC data that was collected during a SHARK flight is shown in Figure 4. The

254   data was from a sampling event in the High Arctic in the summer of 2018, during which the meteorological data

255   from the radiosonde and aerosol particle data from the OPC were collected alongside impactor films for INP

256   analysis (the INP results will be published elsewhere). Throughout the 4.5 h flight the altitude, humidity and

257   temperature were closely monitored to inform decisions on sampling. The sampling start and end times are

258   indicated as solid lines in Figure 4. The SHARK reached 450 m above Mean Sea Level (MSL) and in the last hour

259   of flight lowered to 350 m due to ice formation on the balloon, instrument and tether. The RH during the flight

260   was monitored to ensure the SHARK did not sample in humidity approaching saturation; the impactor and OPC

261   manufacturers' specified thresholds for the components is 95 % RH, but we aim to only sample with the RH below

262   this value (~80 %) in order to reduce the influence of hygroscopic growth on aerosol size. After sampling was

263   stopped, the SHARK was brought down to ground level, resulting in the humidity rising. The ability to stop the

264   sampling during the flight meant the impactors were covered and the pumps turned off during the descent and so

265   did not sample the more humid environment. The ambient temperature was monitored alongside the dewpoint

266   temperature to follow the surface inversions. The temperature inversion was used to determine where to stabilise

267   the SHARK and begin sampling, as sampling was desired above the surface inversion for this run.

268

269   The total particle counts per 1.38 s interval from the OPC are shown in Figure 4d. Processing of the OPC data

270   yielded the results shown in Figure 5 for the particle number ($dN/d\log D_p$), particle surface area ($dS/d\log D_p$) and

271   particle mass ($dM/d\log D_p$) size distribution data for the sampling period, where D_p is the particle diameter. We

272   present this data to demonstrate that the OPC produces reasonable data when used facing into wind while

273   suspended from a balloon at altitude. Unfortunately, there is no direct comparison with other aerosol size

274   distribution measurements at the sampling location. While the particle number concentration decreases roughly

275   linearly with size, the surface and mass concentration curves have a mode at around 4 µm in Figure 5b and 5c.

276   This is consistent with previous studies conducted within the boundary layer in the Arctic (Freud et al., 2017;

277   Hegg et al., 1996; Seinfeld and Pandis, 2016).

278

279   ## 3.2   Deriving size-resolved INP concentrations from the SHARK samples

280   The ability to measure INP concentrations and properties using samples collected via the SHARK was tested by

281   performing immersion mode droplet freezing assays on the sampled aerosols. Following a flight, impactor films

282   were removed from both cascade impactors of the SHARK, then each immersed in 5 mL of water and mixed on

283   a vortex mixer for 5 min to wash the collected particles into suspension (O'Sullivan et al., 2018). This suspension

284   was then analysed via a droplet freezing assay using the microlitre Nucleation by Immersed Particle Instrument

285   (µL-NIPI) (Whale et al., 2015), in which 40-50 droplets of 1 µL volume were pipetted onto a hydrophobic glass

286   slide atop a cold plate. A Perspex shield was placed over the cold stage and N_2 gas introduced to purge the chamber

287   of moisture as the cold plate was cooled to −40 °C at 1 °C min^{-1}. The temperatures at which droplets froze were

288   recorded using video analysis until the entire population had frozen. This allowed the fraction of droplets frozen

289   as a function of temperature, $f_{ice}(T)$, to be calculated (O'Sullivan et al., 2018; Whale et al., 2015) using the equation

290    $f_{ice}(T) = N_f / N_t$, where N_f is the number of frozen droplets at temperature T, and N_t is the total number of droplets.

291   The INP concentration per volume of sampled air as a function of temperature, $[INP]_T$, was then calculated for

292   each film using $f_{ice}(T)$, according to Equation 1 adapted from (Vali, 1971) to include weighting to the volume of

293   air sampled:

294    $$[INP]_T = -\frac{\ln(1 - f_{ice}(T))}{V_{droplet}} \cdot \frac{V_{wash}}{V_{air}} , \tag{1}$$

295   where $V_{droplet}$ is the droplet volume (i.e. 1 µL), V_{wash} is the amount of water into which the filter is immersed to

296   produce the suspension for analysis (i.e. 5 mL), and V_{air} is the volume of air sampled.

297

298   ## 3.3   Testing the SHARK INP concentrations against a standard aerosol sampler

299   In order to test whether the SHARK impactors were sampling in a representative manner, the SHARK was run

300   concurrently with a filter-based particle sampler (BGI PQ100, Mesa Labs) and which is used as an EPA Federal

301   Reference Method for PM$_{10}$ (designation no. RFPS-1298-124). This sampler was equipped with a PM10 head and

302   an optional cyclone impactor which provided a size cut at 2.5 µm. Aerosol was collected onto 0.4 µm pore size

303 Nuclepore Track-Etched Membrane polycarbonate filters at a flow rate of 16.7 L min^{-1} (i.e. 1 m^3 h^{-1}). This type

304 of filter collects particles across the full range of available aerosol sizes, even at sizes smaller than the pore

305 diameter, with high collection efficiencies (Lindsley, 2016; Soo et al., 2016). These polycarbonate filters have

306 also been successfully employed in other ice nucleation field measurements (DeMott et al., 2016; Harrison et al.,

307 2018; Huffman et al., 2013; McCluskey et al., 2016; Reicher et al., 2019; Tarn et al., 2018). These substrates are

308 known to have a low ice-nucleating ability and allow the collected particles to be released into suspension for

309 subsequent INP analysis (O'Sullivan et al., 2018). The filters were analysed using the μL-NIPI in the same manner

310 as for the impactor films collected using the SHARK. The PQ100 filter sampler was deployed alongside the

311 SHARK in Cardington (UK) and in Hyytiälä (Finland).

312

313 In order to compare the SHARK-derived, size-resolved INP data with the results of the PM$_{10}$ or PM$_{2.5}$ PQ100

314 filter sampler, the INP concentrations determined across the appropriate SHARK size categories were summed.

315 In Figure 6a, data is presented from Cardington, where the sum of 2d and 2e from SHARK is compared with the

316 filter sampler fitted with a PM$_{10}$ head (Impactor 1 was not available during this test). The SHARK was suspended

317 from a tethered balloon roughly 20 m from the ground, whereas the filter sampler was on the ground (inlet ~150

318 cm above the surface), where both samplers were within the well-mixed boundary layer. The agreement is very

319 good apart from two highest temperature points from the filter sampler, but note that the Poisson uncertainties on

320 these points are substantial and also that the two samplers were separated vertically by 20 m.

321

322 We then show data from Hyytiälä in Figure 6b where we compare the INP spectrum from the filter sampler, with

323 a PM$_{2.5}$ cut-off installed, with the sum of stages 1b, 1c and 1d (the after-filter, stage 1a was not used on Impactor

324 1 in this case). Here, both samplers were positioned within a few metres above the ground. Again, the agreement

325 between the SHARK and the filter sampler was very good. For both Cardington and Hyytiälä, the smallest

326 particles (<0.25 μm) were not sampled using the SHARK, but the agreement between the filter sampler and the

327 SHARK implies that, in these cases, the smallest particles made a minor contribution to the overall INP

328 population, which is what we would generally anticipate from the literature (Berezinski et al., 1988; Huffman et

329 al., 2013; Mason et al., 2016; Santachiara et al., 2010; Si et al., 2018; Welti et al., 2009). The consistency between

330 the SHARK and the filter sampler indicates that there are no major losses of aerosol in the SHARK sampler, at

331 least relative to the PQ100 filter sampler.

332

333 **3.4   Consistency of INP concentrations between SHARK impactors**

334 An example of data from the size-resolved collection and analysis of INPs is shown in Figure 7, from a sampling

335 run performed in Leeds (UK). The $f_{ice}(T)$ curves for each impactor stage are illustrated in Figure 7a. As discussed

336 in section 2.2, there are two stages, d and e, which have similar size cuts on both stages. Using stage e as an

337 example, it can be seen that while the fraction frozen curves for the two samplers are shifted by about 3 °C (Figure

338 7a), normalising to the volume of air sampled to yield [INP]$_T$ in Figure 7b shows that the INP spectra derived

339 from stages 1e and 2e are consistent with one another. Stage 2e covers a lower range of INP concentrations than

340 stage 1e by about 1 order of magnitude, because the flow rate through this impactor was more than a factor of

341 11.1 (100 L min^{-1} / 9 L min^{-1}) higher and the probability of collecting rarer INP was increased by this factor. The

342 agreement between the two impactors indicates that aerosol was collected with no significant losses/enhancements

343 due to factors like particle bounce or wind observed. Based on the inlet particle loss calculations in Figure 3,

344 higher losses may have been expected in impactor stage 1e, but these are not apparent here.

345

3.5 Size-resolved ice-nucleating particle (srINP) spectra at four locations

347 The derived size-resolved INP (srINP) concentrations for all four test sites are shown in Figure 8 and Figure 9.

348 The $f_{ice}(T)$ curves for these test sites can be found in Figures S1 to S4 of the SI. Figure 8 shows the INP

349 concentration spectra in the classic form, wherein INP concentrations are plotted against temperature for each size

350 bin, whereas Figure 9 shows the same data in novel srINP plots to allow more intuitive comparison of the INP

351 concentration contribution from each stage with respect to temperature. In Figure 9, where there were

352 measurements from two impactors for the same stage (e.g. d and e), the INP concentrations were merged by taking

353 an average at temperature intervals of 0.5 °C (also for Figure 6). The colour gradient in Figure 9 represents the

354 temperature dependant concentration for each size bin and the overall steepness of the d$[INP]_T$/dT curve. The

355 steepness of the INP spectra can be useful in discriminating between different INP species. On inspection of

356 Figure 8 and Figure 9, it can be seen that the spectra in the four locations have very different characteristics. Not

357 only does the general shape of the spectra vary, but the size-dependence is also very different in the four locations.

358 Due to the sample size, these variations could be attributed to the different aerosol population in each location,

359 the time of year and meteorology, which could affect the INP concentrations and spectra (Kanji et al., 2017; Šantl-

360 Temkiv et al., 2019; Tobo et al., 2019; Wex et al., 2019). We now discuss the size-resolved INP concentration

361 spectra from these tests, bearing in mind that these four tests were one-offs and should not be regarded as

362 characteristic of those sampling sites, but rather illustrative of the importance of making size-resolved

363 measurements.

364

365 The first site testing of a prototype of the SHARK in which all of the components were installed was conducted

366 in Cardington (UK) on the 15th of May 2018, but only Impactor 2 was used (see Figure 6a and Figure 8a). The

367 Cardington site is an airfield, with large areas of grassy land near a main road, and the sampling was conducted

368 during spring. In order to demonstrate the utility of the SHARK to make balloon-borne INP measurements whilst

369 providing a comparison with a commercial ground-based sampler, the SHARK was sampling whilst suspended

370 from a tethered balloon, flying roughly 20 m above the ground. The INP spectra (Figure 8a and 9a) in this location

371 are steep, increasing two orders of magnitude within 2.5 °C, and are centred around −18 to −20 °C; the $[INP]_T$ for

372 2f and 2e increases by an order of magnitude in just ~1 °C. The INPs in this location were dominated by particles

373 greater than 2.5 μm, whereas particles between 1-2.5 μm made a smaller contribution and show a shallower

374 d$[INP]_T$/dT, seen in Figure 9a as a larger spread of data. We speculate that the coarse mode INPs at this site were

375 of biological origin, such as fungal material, pollen or bacteria with a steep INP spectrum (Kanji et al., 2017).

376 Some fertile and agricultural soil samples have also been shown to be very active (Hill et al., 2016; O'Sullivan et

377 al., 2015; Steinke et al., 2016; Tobo et al., 2014), and a mechanism for emissions of soil material into the

378 atmosphere has been proposed (Wang et al., 2016). However, the steep portion of the INP spectrum for fertile

379 soils tends to be at temperatures above ~-10°C, warmer than observed in the Cardington sample. The steepness

380 of the curve and the temperature are consistent with ice nucleation by pollen (O'Sullivan et al., 2015; Pummer et

381   al., 2012; Tarn et al., 2018). Although the size of whole pollen grains are often larger than 10 μm, pollen is known

382   to release nanoscale materials that nucleate ice, which might be internally mixed with aerosol in this size bin.

383

384   In Hyytiälä (Finland), a field site in the boreal forest, the INP spectra contrast quite strongly with those in

385   Cardington (see Figure 6b and Figure 8b). Sampling took place on the 11th of March 2018, when the Hyytiälä site

386   was snow-covered and sampling was performed at the surface (inlet ~150 cm above surface). In this case only

387   Impactor 1 was used without the after-filter installed. The complex nature of the size-dependence of INP is clear

388   here. Intriguingly, in this location, the INP concentration was greatest for the smallest stage used (1*b*; 0.25-0.5

389   μm), and accounted for the majority of the INPs between −17 and −22 °C. The fewest INP came from the next

390   smallest stage 1*c* (0.5-1 μm), while at temperatures below −23 °C, stage 1*e* contained the majority of the INPs.

391   These results indicate that the INP spectra are complex, and that concentrations of INPs do not always increase

392   with increasing size as might be expected. Huffman et al. (2013) reported INP concentration measurements in a

393   forest ecosystem, where the particles between 1.8 and 5.6 μm enhanced during rain. Hence, as in the present study,

394   Huffman et al. (2013) showed that INP activity does not always increase with size. The highest INP concentrations

395   in Hyytiälä were measured for aerosol sizes of 0.25-0.5 μm, and we note that these accumulation mode INPs

396   would have lifetimes of many days to weeks in the atmosphere and could therefore be transported to locations and

397   altitudes where they may influence clouds. Clearly, this would be an interesting location for more measurements

398   with the full SHARK payload to gain further information on the long term INP concentration variations and the

399   aerosol sizes responsible for them.

400

401   The testing in Leeds (UK) used both impactors at ground level with the SHARK suspended from a frame to allow

402   orientation into wind. The Leeds sampling was conducted within the University of Leeds campus on a patch of

403   grass on the 7th of June 2018 in close proximity to the School of Earth and Environment. In this test the full suite

404   was deployed, including the impactors, after-filter and OPC. The particle number, surface and mass size

405   distribution data for this test can be found in Figures S5 to S7 of the SI. It can be seen in Figure 8c that generally,

406   the larger bins contained more active INP. The only exception to this occurred with the after-filter (< 0.25 μm),

407   which had slightly higher INP concentrations below about −25 °C than the next two size bins (0.25-1.0 μm). As

408   with the measurements in Hyytiälä, clearly more measurements illuminating the contribution of the smaller

409   particles in similar environments would be beneficial since the atmospheric lifetime of these fine particles is

410   relatively long. We note that a substantial proportion of INPs quantified just outside of Leeds in a previous study

411   were heat-sensitive and therefore most likely of biological origin (O'Sullivan et al. 2018). In the future, conducting

412   heat tests, as well as using Mass Spectrometry, SEM and DNA analysis with the size-resolved INP samples may

413   help to identify the INP types in the various size fractions and highlight any differences between size ranges.

414

415   The final test was in Longyearbyen (Svalbard) from the 7th deck of the icebreaker Oden, 25 m above the surface,

416   when moored ~200 m from the shore, overnight from the 23rd to the 24th of September 2018. The full SHARK

417   payload was used in this case, with the OPC, both impactors and the after-filter on Impactor 1. The particle

418   number, surface and mass size distribution data for this test can be found in Figures S8 to S10 of the SI. The INP

419   spectra in this location, shown in Figure 8d was quite distinct from the other three locations in that all size fractions

420   contributed similarly to the INP population and there is a very shallow slope of $d\ln[INP]_T/dT$ (Figure 9d). We

421   detected INPs at temperatures of up to −10 °C with concentrations of around 0.01 INP L^{-1}. These high-temperature

422   INP concentrations are consistent with the summertime measurements reported at other Arctic locations, including

423   Ny-Ålesund (Svalbard) (Wex et al., 2019). The INP in this region potentially originate from a range of sources.

424   Tobo et al. (2019) recently reported that dust and biological material from glacial valleys in Svalbard may be an

425   important source of INPs in the region. We also note that we sampled while the Oden was moored in the port of

426   Longyearbyen where local pollution sources may have been significant (Zhao et al., 2019).

427

3.6   Ice-active surface site density, $n_s(T)$, and the activated fraction, $n_n(T)$

429   The addition of size distribution information to the INP concentration spectra allowed the calculation of the

430   number of active sites per unit surface area, $n_s(T)$, and the activated fraction, $n_n(T)$, of the size-resolved samples.

431   These quantities are determined by weighting the srINP concentrations to the total surface area and the aerosol

432   number in each size bin, respectively, as shown in Equations 2 and 3.

433    $$n_s(T) = -\frac{\ln(1 - f_{\text{ice}}(T))}{A_s},\qquad(2)$$

434   where A_s is the total surface area of the particles per droplet in a μL-NIPI droplet freezing assay. This was

435   calculated for each impactor size range, using data from the relevant size bins of the OPC data.

436    $$n_n(T) = -\frac{\ln(1 - f_{\text{ice}}(T))}{N},\qquad(3)$$

437   where N is the total number of particles sampled by the impactor in each size bin, calculated using the number

438   concentration in each size category as measured by the OPC, and the volume of air sampled by the impactor. The

439   size bins from the OPC which have been included in the calculations were matched to those in the impactors. The

440   bin boundaries for the OPC calculations were within tens of nanometres of the impactor bin boundaries.

441

442   Calculating the $n_s(T)$ and $n_n(T)$ values from the INP data was only possible for some of the size ranges due to the

443   sampling ranges of the instrumentation employed. The smallest particle diameter measured by the OPC is 0.38

444   μm, i.e. above the lower limit of impactor stage 1b, while the largest impactor stage, 2f (>10 μm) has no defined

445   upper bound. Therefore, the three bins (i.e. impactor stages) that were used to produce $n_s(T)$ and $n_n(T)$ were c (0.5-

446   1.0 μm), d (1.0-2.5 μm) and e (2.5-10 μm). The $n_s(T)$ and $n_n(T)$ data were calculated for the field tests in Leeds

447   and Longyearbyen; data from Cardington and Hyytiälä is not provided as the OPC was not in use at these sites.

448

449   The plots of activated fraction shown in Figure 10 are addressed first. For the Leeds sample, there is a difference

450   in the $n_n(T)$ values between bins c to e (Figure 10a), where the smallest bin is 1-3 orders of magnitude lower than

451   the largest bin, with the middle bin in the centre of the two. In Longyearbyen (Figure 10b), the $n_n(T)$ for bin e is

452   about a factor of 10 larger than bin c, but bins c and d produce very similar values of $n_n(T)$. Overall, these $n_n(T)$

453   plots show that the coarse mode aerosol generally have a higher fraction of aerosol that serve as INPs than the

454   fine mode, but there is variability in the dependence on size between the two samples. In contrast to the $n_n(T)$

455   values, the size resolved $n_s(T)$ data for both Leeds and Longyearbyen show that the data from the three size

456   categories are all within a factor of 2-10 (close to our uncertainty estimates). Given the activity of aerosol across

457   these bins scales with surface area, this data might indicate the same INP species is active across each bin at these

458   sites.

4   Conclusions

This paper describes a lightweight and portable payload, the SHARK, that is capable of collecting size-resolved aerosol particles alongside measurements of ambient temperature, relative humidity, pressure, GPS coordinates, aerosol number distribution and aerosol size distribution. The 9 kg payload was designed for use on a tethered balloon for measurements at user-selected altitudes for up to 11 h via radio controlled instrumentation, but can be used wherever it can be suspended. During a SHARK flight, the atmospheric conditions the SHARK experiences can be monitored in real-time via a radiosonde and sampling is controlled remotely, allowing the SHARK to be held at a user-defined height and to only sample under specific conditions (for instance above the surface boundary layer).

The SHARK samples aerosol onto filter/film substrates using two cascade impactors to allow aerosol size-segregation from 0.25 to 10 µm, with an after-filter and top stage to collect particles below and above this range. One impactor samples at 9 L min^{-1}, while the other samples at 100 L min^{-1}. The filters were collected here for the offline analysis of INP concentrations and properties, but they could equally be used for other analyses such as mass spectrometry, DNA analysis, SEM, TEM and ion chromatography. A comparison of ambient INP concentrations measured using the SHARK to those measured using PM$_{10}$ and PM$_{2.5}$ aerosol samplers at ground level demonstrated excellent agreement between the instruments. Field testing was conducted in four locations close to ground level, and suspended on a tethered balloon at 20 m to demonstrate the capabilities of the SHARK.

The size resolved INP concentration spectra reveal complex behaviour. For example in Hyytiälä the 0.25-0.5 µm aerosol size fraction had the most active INP, whereas in Leeds the INP concentration generally decreased with decreasing particle size. Ambient aerosol size distribution measured using the on-board OPC allowed the calculation of the activated fraction ($n_n(T)$) and ice-active surface site density ($n_s(T)$) data for the sampled INPs in the tests at Leeds and Longyearbyen. It was shown that $n_s(T)$ was consistent between 0.5 and 10 µm in these two locations at the times of sampling. It is the intention to make similar measurements in other locations, and at higher altitudes in the future.

Generally, it is expected that larger aerosol are more likely to nucleate ice (Pruppacher, H.R. and Klett, 1997) and our results are consistent with other size resolved INP measurements which indicate that the size distribution of INP varies spatially and temporarily e.g. (Mason et al., 2016; Si et al., 2018). Quantifying the size of INP, possibly in conjunction with other analytical techniques, is a useful means of identifying different INP types and their sources (Huffman et al., 2013). In addition, knowledge of their size will allow the improved representation of INP in global aerosol models where size is key determinant of lifetime and transport (Atkinson et al., 2013; Perlwitz et al., 2015; Vergara-Temprado et al., 2017). Clearly, more systematic and widespread measurements of INP size is needed in the future in a range of target locations.

The high sample flow rate, choice of low contamination aerosol collection substrates and long sampling durations mean that the payload is well suited for INP measurements, including those in low aerosol environments and locations with relatively low INP concentrations (down to below ~0.01 INP L^{-1} and at temperatures down to about −25 °C and below).   The SHARK is an accessible tool for quantifying size-resolved atmospheric INP

499 concentrations from a tethered balloon.. This will allow improved determination of INP sizes, properties, and
500 sources, towards ultimately improving model representations of atmospheric INP distributions.

Data availability

502 The data sets for this paper will be made publicly available in the University of Leeds Data Repository upon
503 publication.

Author contribution

505 GCEP led the development of the SHARK, performed the bulk of the experiments and led the writing of the paper.
506 The initial instrument concept was conceived by GCEP, SNFS and BJM with advice from IMB. The building and
507 testing of the SHARK and its electrical components was done by SNFS with the assistance of GCEP. The
508 collection and analysis of field samples was performed by GCEP, MPA, UP, ADH, MDT and IMB. All authors
509 contributed to the writing of this paper. BJM oversaw this project as part of his MarineIce ERC fellowship.

Competing interest

511 The authors declare that they have no conflict of interest.

Acknowledgements

513 The personnel of Hyytiälä forestry station, the HyIce project team, the Cardington meteorological research unit,
514 and those aboard the icebreaker Oden during 2018 are sincerely thanked for support during field testing. One of
515 the field tests was completed as part of the Arctic Ocean (AO) 2018 expedition. The Swedish Polar Research
516 Secretariat (SPRS) provided access to the icebreaker Oden and logistical support in collaboration with the U.S.
517 National Science Foundation. We are grateful to the Chief Scientists Caroline Leck and Patricia Matrai for
518 planning and coordination of AO2018, as well as to the SPRS logistical staff and icebreaker Oden's Captain
519 Mattias Peterson and his crew for expert field support. The authors thank the European Research Council for
520 funding (H2020 ERC; 648661 MarineIce) and the Natural Environment Research Council (NERC,
521 NE/M010473/1, NE/R009686/1). We are grateful to the EU's H2020 ACTRIS-2 for a mobility grant to access
522 the Hyytiälä forestry station as part of the HyIce project (SMR7 RP3 HyICE18, 654109). Anthony Windross and
523 Stephen Burgess are thanked for help with the fabrication of the SHARK housing.
524

References

Armstrong, J. A., Russell, P. A., Sparks, L. E. and Drehmel, D. C.: Tethered Balloon Sampling Systems for Monitoring Air Pollution, J. Air Pollut. Control Assoc., 31(7), 735–743, doi:10.1080/00022470.1981.10465268, 1981.

Atkinson, J. D., Murray, B. J., Woodhouse, M. T., Whale, T. F., Baustian, K. J., Carslaw, K. S., Dobbie, S., O'Sullivan, D., Malkin, T. L., O 'sullivan, D. and Malkin, T. L.: The importance of feldspar for ice nucleation by mineral dust in mixed-phase clouds., Nature, 498(7454), 355–8, doi:10.1038/nature12278, 2013.

Ault, A. P. and Axson, J. L.: Atmospheric Aerosol Chemistry: Spectroscopic and Microscopic Advances, Anal. Chem., 89(1), 430–452, doi:10.1021/acs.analchem.6b04670, 2017.

Balsley, B. B., Jensen, M. L. and Frehlich, R. G.: The use of state-of-the-art kites for profiling the lower atmosphere, Boundary-Layer Meteorol., 87(1), 1–25, doi:10.1023/A:1000812511429, 1998.

Berezinski, N. A., Stepanov, G. V. and Khorguani, V. G.: Ice-forming activity of atmospheric aerosol particles of different sizes, Atmos. Aerosols Nucleation, 309, 709–712, doi:https://doi.org/10.1007/3-540-50108-8_1167, 1988.

Cheng, Y.-S. and Yeh, H.-C.: Particle bounce in cascade impactors., Environ. Sci. Technol., 13(11), 1392–1396, doi:10.1021/es60159a017, 1979.

Conen, F., Rodríguez, S., Hülin, C., Henne, S., Herrmann, E., Bukowiecki, N., Alewell, C., Rodri´guez, S., Rodri´guez, R., Hu¨glin, C. and Hu¨glin, H.: Atmospheric ice nuclei at the high-altitude observatory Jungfraujoch, Chem. Phys. Meteorol., 67(1), doi:10.3402/tellusb.v67.25014, 2015.

Creamean, J. M., Primm, K., Tolbert, M. A., Hall, E. G., Wendell, J., Jordan, A., Sheridan, P. J., Smith, J. and Schnell, R. C.: HOVERCAT: A novel aerial system for evaluation of aerosol-cloud interactions, Atmos. Meas. Tech., 11(7), 3969–3985, doi:10.5194/amt-11-3969-2018, 2018a.

Creamean, J. M., Kirpes, R. M., Pratt, K. A., Spada, N. J., Maahn, M., De Boer, G., Schnell, R. C. and China, S.: Marine and terrestrial influences on ice nucleating particles during continuous springtime measurements in an Arctic oilfield location, Atmos. Chem. Phys., 18(24), 18023–18042, doi:10.5194/acp-18-18023-2018, 2018b.

DeMott, P. J., Prenni, A. J., Liu, X., Kreidenweis, S. M., Petters, M. D., Twohy, C. H., Richardson, M. S., Eidhammer, T. and Rogers, D. C.: Predicting global atmospheric ice nuclei distributions and their impacts on climate, Proc. Natl. Acad. Sci., 107(25), 11217–11222, doi:10.1073/pnas.0910818107, 2010.

DeMott, P. J., Prenni, A. J., McMeeking, G. R., Sullivan, R. C., Petters, M. D., Tobo, Y., Niemand, M., Möhler, O., Snider, J. R., Wang, Z. and Kreidenweis, S. M.: Integrating laboratory and field data to quantify the immersion freezing ice nucleation activity of mineral dust particles, Atmos. Chem. Phys., 15(1), 393–409, doi:10.5194/acp-15-393-2015, 2015.

DeMott, P. J., Hill, T. C. J., McCluskey, C. S., Prather, K. A., Collins, D. B., Sullivan, R. C., Ruppel, M. J., Mason, R. H., Irish, V. E., Lee, T., Hwang, C. Y., Rhee, T. S., Snider, J. R., McMeeking, G. R., Dhaniyala, S., Lewis, E. R., Wentzell, J. J. B., Abbatt, J., Lee, C., Sultana, C. M., Ault, A. P., Axson, J. L., Diaz Martinez, M., Venero, I., Santos-Figueroa, G., Stokes, M. D., Deane, G. B., Mayol-Bracero, O. L., Grassian, V. H., Bertram, T.

561   H., Bertram, A. K., Moffett, B. F. and Franc, G. D.: Sea spray aerosol as a unique source of ice nucleating particles,
562   Proc. Natl. Acad. Sci., 113(21), 5797–5803, doi:10.1073/pnas.1514034112, 2016.

563   DeMott, P. J., Hill, T. C. J., Petters, M. D., Bertram, A. K., Tobo, Y., Mason, R. H., Suski, K. J., Mccluskey, C.
564   S., Levin, E. J. T., Schill, G. P., Boose, Y., Rauker, A. M., Miller, A. J., Zaragoza, J., Rocci, K., Rothfuss, N. E.,
565   Taylor, H. P., Hader, J. D., Chou, C., Huffman, J. A., Pöschl, U., Prenni, A. J. and Kreidenweis, S. M.:
566   Comparative measurements of ambient atmospheric concentrations of ice nucleating particles using multiple
567   immersion freezing methods and a continuous flow diffusion chamber, Atmos. Chem. Phys., 17(18), 11227–
568   11245, doi:10.5194/acp-17-11227-2017, 2017.

569   Deng, X., Xue, H. and Meng, Z.: The effect of ice nuclei on a deep convective cloud in South China, Atmos. Res.,
570   206, 1–12, doi:10.1016/j.atmosres.2018.02.013, 2018.

571   Dzubay, T. G., Hines, L. E. and Stevens, R. K.: Particle bounce errors in cascade impactors, Atmos. Environ.,
572   10(3), 229–234, doi:10.1016/0004-6981(76)90095-0, 1976.

573   Freud, E., Krejci, R., Tunved, P., Leaitch, R., Nguyen, Q. T., Massling, A., Skov, H. and Barrie, L.: Pan-Arctic
574   aerosol number size distributions: Seasonality and transport patterns, Atmos. Chem. Phys., 17(13), 8101–8128,
575   doi:10.5194/acp-17-8101-2017, 2017.

576   Garcia, E., Hill, T. C. J., Prenni, A. J., DeMott, P. J., Franc, G. D. and Kreidenweis, S. M.: Biogenic ice nuclei in
577   boundary layer air over two U.S. High Plains agricultural regions, J. Geophys. Res. Atmos., 117(D18), n/a-n/a,
578   doi:10.1029/2012JD018343, 2012.

579   Hara, K., Osada, K. and Yamanouchi, T.: Tethered balloon-borne aerosol measurements: Seasonal and vertical
580   variations of aerosol constituents over Syowa Station, Antarctica, Atmos. Chem. Phys., 13(17), 9119–9139,
581   doi:10.5194/acp-13-9119-2013, 2013.

582   Harrison, A. D., Whale, T. F., Rutledge, R., Lamb, S., Tarn, M. D., Porter, G. C. E., Adams, M. P., McQuaid, J.
583   B., Morris, G. J. and Murray, B. J.: An instrument for quantifying heterogeneous ice nucleation in multiwell plates
584   using infrared emissions to detect freezing, Atmos. Meas. Tech., 11(10), 5629–5641, doi:10.5194/amt-11-5629-
585   2018, 2018.

586   Hegg, D. A., Hobbs, P. V, Gassó, S., Nance, J. D. and Rangno, A. L.: Aerosol measurements in the Arctic relevant
587   to direct and indirect radiative forcing, J. Geophys. Res. Atmos., 101(D18), 23349–23363,
588   doi:10.1029/96jd02246, 1996.

589   Herbert, R. J., Murray, B. J., Dobbie, S. J. and Koop, T.: Sensitivity of liquid clouds to homogenous freezing
590   parameterizations, Geophys. Res. Lett., 42(5), 1599–1605, doi:10.1002/2014GL062729, 2015.

591   Hill, T. C. J., Demott, P. J., Tobo, Y., Fröhlich-Nowoisky, J., Moffett, B. F., Franc, G. D. and Kreidenweis, S. M.:
592   Sources of organic ice nucleating particles in soils, Atmos. Chem. Phys., 16(11), 7195–7211, doi:10.5194/acp-
593   16-7195-2016, 2016.

594   Huffman, J. A., Prenni, A. J., Demott, P. J., Pöhlker, C., Mason, R. H., Robinson, N. H., Fröhlich-Nowoisky, J.,
595   Tobo, Y., Després, V. R., Garcia, E., Gochis, D. J., Harris, E., Müller-Germann, I., Ruzene, C., Schmer, B., Sinha,
596   B., Day, D. A., Andreae, M. O., Jimenez, J. L., Gallagher, M., Kreidenweis, S. M., Bertram, A. K., Pöschl, U., M

561   H., Bertram, A. K., Moffett, B. F. and Franc, G. D.: Sea spray aerosol as a unique source of ice nucleating particles,
562   Proc. Natl. Acad. Sci., 113(21), 5797–5803, doi:10.1073/pnas.1514034112, 2016.

563   DeMott, P. J., Hill, T. C. J., Petters, M. D., Bertram, A. K., Tobo, Y., Mason, R. H., Suski, K. J., Mccluskey, C.
564   S., Levin, E. J. T., Schill, G. P., Boose, Y., Rauker, A. M., Miller, A. J., Zaragoza, J., Rocci, K., Rothfuss, N. E.,
565   Taylor, H. P., Hader, J. D., Chou, C., Huffman, J. A., Pöschl, U., Prenni, A. J. and Kreidenweis, S. M.:
566   Comparative measurements of ambient atmospheric concentrations of ice nucleating particles using multiple
567   immersion freezing methods and a continuous flow diffusion chamber, Atmos. Chem. Phys., 17(18), 11227–
568   11245, doi:10.5194/acp-17-11227-2017, 2017.

569   Deng, X., Xue, H. and Meng, Z.: The effect of ice nuclei on a deep convective cloud in South China, Atmos. Res.,
570   206, 1–12, doi:10.1016/j.atmosres.2018.02.013, 2018.

571   Dzubay, T. G., Hines, L. E. and Stevens, R. K.: Particle bounce errors in cascade impactors, Atmos. Environ.,
572   10(3), 229–234, doi:10.1016/0004-6981(76)90095-0, 1976.

573   Freud, E., Krejci, R., Tunved, P., Leaitch, R., Nguyen, Q. T., Massling, A., Skov, H. and Barrie, L.: Pan-Arctic
574   aerosol number size distributions: Seasonality and transport patterns, Atmos. Chem. Phys., 17(13), 8101–8128,
575   doi:10.5194/acp-17-8101-2017, 2017.

576   Garcia, E., Hill, T. C. J., Prenni, A. J., DeMott, P. J., Franc, G. D. and Kreidenweis, S. M.: Biogenic ice nuclei in
577   boundary layer air over two U.S. High Plains agricultural regions, J. Geophys. Res. Atmos., 117(D18), n/a-n/a,
578   doi:10.1029/2012JD018343, 2012.

579   Hara, K., Osada, K. and Yamanouchi, T.: Tethered balloon-borne aerosol measurements: Seasonal and vertical
580   variations of aerosol constituents over Syowa Station, Antarctica, Atmos. Chem. Phys., 13(17), 9119–9139,
581   doi:10.5194/acp-13-9119-2013, 2013.

582   Harrison, A. D., Whale, T. F., Rutledge, R., Lamb, S., Tarn, M. D., Porter, G. C. E., Adams, M. P., McQuaid, J.
583   B., Morris, G. J. and Murray, B. J.: An instrument for quantifying heterogeneous ice nucleation in multiwell plates
584   using infrared emissions to detect freezing, Atmos. Meas. Tech., 11(10), 5629–5641, doi:10.5194/amt-11-5629-
585   2018, 2018.

586   Hegg, D. A., Hobbs, P. V, Gassó, S., Nance, J. D. and Rangno, A. L.: Aerosol measurements in the Arctic relevant
587   to direct and indirect radiative forcing, J. Geophys. Res. Atmos., 101(D18), 23349–23363,
588   doi:10.1029/96jd02246, 1996.

589   Herbert, R. J., Murray, B. J., Dobbie, S. J. and Koop, T.: Sensitivity of liquid clouds to homogenous freezing
590   parameterizations, Geophys. Res. Lett., 42(5), 1599–1605, doi:10.1002/2014GL062729, 2015.

591   Hill, T. C. J., Demott, P. J., Tobo, Y., Fröhlich-Nowoisky, J., Moffett, B. F., Franc, G. D. and Kreidenweis, S. M.:
592   Sources of organic ice nucleating particles in soils, Atmos. Chem. Phys., 16(11), 7195–7211, doi:10.5194/acp-
593   16-7195-2016, 2016.

594   Huffman, J. A., Prenni, A. J., Demott, P. J., Pöhlker, C., Mason, R. H., Robinson, N. H., Fröhlich-Nowoisky, J.,
595   Tobo, Y., Després, V. R., Garcia, E., Gochis, D. J., Harris, E., Müller-Germann, I., Ruzene, C., Schmer, B., Sinha,
596   B., Day, D. A., Andreae, M. O., Jimenez, J. L., Gallagher, M., Kreidenweis, S. M., Bertram, A. K., Pöschl, U., M

¨Uller-Germann, I., Ruzene, C., Schmer, B., Sinha, B., Day, D. A., Andreae, M. O., Jimenez, J. L., Gallagher, M., Kreidenweis, S. M., Bertram, A. K. and Pöschl, U.: High concentrations of biological aerosol particles and ice nuclei during and after rain, Atmos. Chem. Phys., 13(13), 6151–6164, doi:10.5194/acp-13-6151-2013, 2013.

Jacob, J., Chilson, P., Houston, A., Smith, S., Jacob, J. D., Chilson, P. B., Houston, A. L. and Smith, S. W.: Considerations for Atmospheric Measurements with Small Unmanned Aircraft Systems, Atmosphere (Basel)., 9(7), 252, doi:10.3390/atmos9070252, 2018.

Jaenicke, R.: Aerosol Physics and Chemistry. In: Landolt-Börnstein Numerical Data and Functional Relationships in Science and Technology New Series Group V: Geophysics and Space Research Volume 4 Meteorology Subvolume b, Physical and Chemical Properties of the Air, edited by G. Fischer., 2007.

Kanitz, T., Seifert, P., Ansmann, A., Engelmann, R., Althausen, D., Casiccia, C. and Rohwer, E. G.: Contrasting the impact of aerosols at northern and southern midlatitudes on heterogeneous ice formation, Geophys. Res. Lett., 38(17), n/a-n/a, doi:10.1029/2011GL048532, 2011.

Kanji, Z. A., Ladino, L. A., Wex, H., Boose, Y., Burkert-Kohn, M., Cziczo, D. J. and Krämer, M.: Overview of Ice Nucleating Particles, Meteorol. Monogr., 58, 1.1-1.33, doi:10.1175/AMSMONOGRAPHS-D-16-0006.1, 2017.

Lacher, L., Steinbacher, M., Bukowiecki, N., Herrmann, E., Zipori, A. and Kanji, Z. A.: Impact of air mass conditions and aerosol properties on ice nucleating particle concentrations at the High Altitude Research Station Jungfraujoch, Atmosphere (Basel)., 9(9), 363, doi:10.3390/atmos9090363, 2018.

Laskin, J., Laskin, A. and Nizkorodov, S. A.: Mass Spectrometry Analysis in Atmospheric Chemistry, Anal. Chem., 90(1), 166–189, doi:10.1021/acs.analchem.7b04249, 2018.

Lindsley, W. G.: Filter Pore Size and Aerosol Sample Collection, in NIOSH Manual of Analytical Methods, pp. 1–14. [online] Available from: https://www.cdc.gov/niosh/docs/2014-151/pdfs/chapters/chapter-fp.pdf (Accessed 30 July 2018), 2016.

Lohmann, U.: Anthropogenic Aerosol Influences on Mixed-Phase Clouds, Curr. Clim. Chang. Reports, 3(1), 32–44, doi:10.1007/s40641-017-0059-9, 2017.

Marple, V. A., Rubow, K. L. and Behm, S. M.: A microorifice uniform deposit impactor (moudi): Description, calibration, and use, Aerosol Sci. Technol., 14(4), 434–436, doi:10.1080/02786829108959504, 1991.

Mason, R. H., Si, M., Chou, C., Irish, V. E., Dickie, R., Elizondo, P., Wong, R., Brintnell, M., Elsasser, M., Lassar, W. M., Pierce, K. M., Leaitch, W. R., MacDonald, A. M., Platt, A., Toom-Sauntry, D., Sarda-Estève, R., Schiller, C. L., Suski, K. J., Hill, T. C. J., Abbatt, J. P. D., Huffman, J. A., DeMott, P. J. and Bertram, A. K.: Size-resolved measurements of ice-nucleating particles at six locations in North America and one in Europe, Atmos. Chem. Phys., 16(3), 1637–1651, doi:10.5194/acp-16-1637-2016, 2016.

McCluskey, C. S., Hill, T. C. J., Malfatti, F., Sultana, C. M., Lee, C., Santander, M. V, Beall, C. M., Moore, K. A., Cornwell, G. C., Collins, D. B., Prather, K. A., Jayarathne, T., Stone, E. A., Azam, F., Kreidenweis, S. M. and DeMott, P. J.: A dynamic link between ice nucleating particles released in nascent sea spray aerosol and oceanic biological activity during two mesocosm experiments, J. Atmos. Sci., JAS-D-16-0087.1, doi:10.1175/JAS-D-16-

0087.1, 2016.

Misra, C., Singh, M., Shen, S., Sioutas, C. and Hall, P. M.: Development and evaluation of a personal cascade impactor sampler (PCIS), Aerosol Sci., 33(7), 1027–1047, doi:10.1016/S0021-8502(02)00055-1, 2002.

Murray, B. J.: Cracking the problem of ice nucleation, Science (80-.)., 355(6323), 346–347, doi:10.1126/science.aam5320, 2017.

Murray, B. J., O'Sullivan, D., Atkinson, J. D. and Webb, M. E.: Ice nucleation by particles immersed in supercooled cloud droplets, Chem. Soc. Rev., 41(19), 6519, doi:10.1039/c2cs35200a, 2012.

O'Sullivan, D., Murray, B. J., Ross, J. F., Whale, T. F., Price, H. C., Atkinson, J. D., Umo, N. S. and Webb, M. E.: The relevance of nanoscale biological fragments for ice nucleation in clouds, Sci. Rep., 5(1), 8082, doi:10.1038/srep08082, 2015.

O'Sullivan, D., Adams, M. P., Tarn, M. D., Harrison, A. D., Vergara-Temprado, J., Porter, G. C. E., Holden, M. A., Sanchez-Marroquin, A., Carotenuto, F., Whale, T. F., McQuaid, J. B., Walshaw, R., Hedges, D. H. P., Burke, I. T., Cui, Z. and Murray, B. J.: Contributions of biogenic material to the atmospheric ice-nucleating particle population in North Western Europe, Sci. Rep., 8(1), 13821, doi:10.1038/s41598-018-31981-7, 2018.

Perlwitz, J. P., Pérez García-Pando, C. and Miller, R. L.: Predicting the mineral composition of dust aerosols-Part 1: Representing key processes, Atmos. Chem. Phys, 15, 11593–11627, doi:10.5194/acp-15-11593-2015, 2015.

Price, H. C., Baustian, K. J., McQuaid, J. B., Blyth, A., Bower, K. N., Choularton, T., Cotton, R. J., Cui, Z., Field, P. R., Gallagher, M., Hawker, R., Merrington, A., Miltenberger, A., Neely, R. R., Parker, S. T., Rosenberg, P. D., Taylor, J. W., Trembath, J., Vergara-Temprado, J., Whale, T. F., Wilson, T. W., Young, G. and Murray, B. J.: Atmospheric Ice-Nucleating Particles in the Dusty Tropical Atlantic, J. Geophys. Res. Atmos., 123(4), 2175–2193, doi:10.1002/2017JD027560, 2018.

Product Information Sheet - MSP: Models 128,129,130 and 131—High Flow Impactors (HFI), [online] Available from: http://www.mspcorp.com/resources/msp-pi-130-revb-us-high-flow-impactors-hfi-128-129-130-131.pdf (Accessed 3 October 2019), n.d.

Pruppacher, H.R. and Klett, J. D.: Microphysics of Clouds and Precipitation, 2nd Editio., Kluwer Academic Publishers, Dordrecht., 1997.

Pummer, B. G., Bauer, H., Bernardi, J., Bleicher, S. and Grothe, H.: Suspendable macromolecules are responsible for ice nucleation activity of birch and conifer pollen, Atmos. Chem. Phys., 12(5), 2541–2550, doi:10.5194/acp-12-2541-2012, 2012.

Rader, D. J. and Marple, V. A.: Effect of Ultra-Stokesian Drag and Particle Interception on Impaction Characteristics, Aerosol Sci. Technol., 4(2), 141–156, doi:10.1080/02786828508959044, 1985.

Reagan, J. A., Apte, M. V., Bruhns, T. V. and Youngbluth, O.: Lidar and Balloon-Borne Cascade Impactor Measurements of Aerosols: A Case Study, Aerosol Sci. Technol., 3(3), 259–275, doi:10.1080/02786828408959014, 1984.

Reicher, N., Segev, L. and Rudich, Y.: The WeIzmann Supercooled Droplets Observation on a Microarray (WISDOM) and application for ambient dust, Atmos. Meas. Tech., 11(1), 233–248, doi:10.5194/amt-11-233-

669   2018, 2018.

670   Reicher, N., Budke, C., Eickhoff, L., Raveh-Rubin, S., Kaplan-Ashiri, I., Koop, T. and Rudich, Y.: Size-dependent
671   ice nucleation by airborne particles during dust events in the Eastern Mediterranean, Atmos. Chem. Phys.
672   Discuss., 1–26, doi:10.5194/acp-2019-511, 2019.

673   Rogers, D. C., Demott, P. J. and Kreidenweis, S. M.: Airborne measurements of tropospheric ice-nucleating
674   aerosol particles in the Arctic spring, J. Geophys. Res., 106(D14), 15053–15063, doi:10.1029/2000JD900790,
675   2001.

676   Rosenfeld, D., Yu, X., Liu, G., Xu, X., Zhu, Y., Yue, Z., Dai, J., Dong, Z., Dong, Y. and Peng, Y.: Glaciation
677   temperatures of convective clouds ingesting desert dust, air pollution and smoke from forest fires, Geophys. Res.
678   Lett., 38(21), n/a-n/a, doi:10.1029/2011GL049423, 2011.

679   Santachiara, G., Di Matteo, L., Prodi, F. and Belosi, F.: Atmospheric particles acting as Ice Forming Nuclei in
680   different size ranges, Atmos. Res., 96(2–3), 266–272, doi:10.1016/j.atmosres.2009.08.004, 2010.

681   Šantl-Temkiv, T., Lange, R., Beddows, D., Rauter, U., Pilgaard, S., Dall'osto, M., Gunde-Cimerman, N.,
682   Massling, A. and Wex, H.: Biogenic Sources of Ice Nucleating Particles at the High Arctic Site Villum Research
683   Station, Environ. Sci. Technol., 53(18), 10580–10590, doi:10.1021/acs.est.9b00991, 2019.

684   Seinfeld, J. H. and Pandis, S. N.: Atmospheric chemistry and physics : from air pollution to climate change, Third
685   edition. [online] Available from: https://www.worldcat.org/title/atmospheric-chemistry-and-physics-from-air-
686   pollution-to-climate-change/oclc/929985301 (Accessed 5 July 2019), 2016.

687   Si, M., Irish, V. E., Mason, R. H., Vergara-Temprado, J., Hanna, S. J., Ladino, L. A., Yakobi-Hancock, J. D.,
688   Schiller, C. L., Wentzell, J. J. B., Abbatt, J. P. D., Carslaw, K. S., Murray, B. J. and Bertram, A. K.: Ice-nucleating
689   ability of aerosol particles and possible sources at three coastal marine sites, Atmos. Chem. Phys, 18, 15669–
690   15685, doi:10.5194/acp-18-15669-2018, 2018.

691   SKC: Leland Legacy Sample Pump: Operating Instructions, , (Form 40075 Rev 1910) [online] Available from:
692   https://www.skcinc.com/catalog/pdf/instructions/40075.pdf (Accessed 25 February 2020), n.d.

693   Soo, J. C., Monaghan, K., Lee, T., Kashon, M. and Harper, M.: Air sampling filtration media: Collection efficiency
694   for respirable size-selective sampling, Aerosol Sci. Technol., 50(1), 76–87, doi:10.1080/02786826.2015.1128525,
695   2016.

696   Steinke, I., Funk, R., Busse, J., Iturri, A., Kirchen, S., Leue, M., Möhler, O., Schwartz, T., Schnaiter, M., Sierau,
697   B., Toprak, E., Ullrich, R., Ulrich, A., Hoose, C. and Leisner, T.: Ice nucleation activity of agricultural soil dust
698   aerosols from Mongolia, Argentina, and Germany, J. Geophys. Res. Atmos., 121(22), 559–576,
699   doi:10.1002/2016JD025160, 2016.

700   Storelvmo, T.: Aerosol Effects on Climate via Mixed-Phase and Ice Clouds, Annu. Rev. Earth Planet. Sci., 45(1),
701   199–222, doi:10.1146/annurev-earth-060115-012240, 2017.

702   Tarn, M. D., Sikora, S. N. F., Porter, G. C. E., O'Sullivan, D., Adams, M., Whale, T. F., Harrison, A. D., Vergara-
703   Temprado, J., Wilson, T. W., Shim, J. uk and Murray, B. J.: The study of atmospheric ice-nucleating particles via
704   microfluidically generated droplets, Microfluid. Nanofluidics, 22(5), doi:10.1007/s10404-018-2069-x, 2018.

Tobo, Y., Prenni, A. J., Demott, P. J., Huffman, J. A., McCluskey, C. S., Tian, G., Pöhlker, C., Pöschl, U. and Kreidenweis, S. M.: Biological aerosol particles as a key determinant of ice nuclei populations in a forest ecosystem, J. Geophys. Res. Atmos., 118(17), 10100–10110, doi:10.1002/jgrd.50801, 2013.

Tobo, Y., DeMott, P. J., Hill, T. C. J., Prenni, A. J., Swoboda-Colberg, N. G., Franc, G. D. and Kreidenweis, S. M.: Organic matter matters for ice nuclei of agricultural soil origin, Atmos. Chem. Phys., 14(16), 8521–8531, doi:10.5194/acp-14-8521-2014, 2014.

Tobo, Y., Adachi, K., Demott, P. J., Hill, T. C. J., Hamilton, D. S., Mahowald, N. M., Nagatsuka, N., Ohata, S., Uetake, J., Kondo, Y. and Koike, M.: Glacially sourced dust as a potentially significant source of ice nucleating particles, Nat. Geosci., 12, doi:10.1038/s41561-019-0314-x, 2019.

Vali, G.: Quantitative Evaluation of Experimental Results an the Heterogeneous Freezing Nucleation of Supercooled Liquids, J. Atmos. Sci., 28(3), 402–409, doi:10.1175/1520-0469(1971)028<0402:qeoera>2.0.co;2, 1971.

Vergara-Temprado, J., Murray, B. J., Wilson, T. W., O'Sullivan, D., Browse, J., Pringle, K. J., Ardon-Dryer, K., Bertram, A. K., Burrows, S. M., Ceburnis, D., Demott, P. J., Mason, R. H., O'Dowd, C. D., Rinaldi, M. and Carslaw, K. S.: Contribution of feldspar and marine organic aerosols to global ice nucleating particle concentrations, Atmos. Chem. Phys., 17(5), 3637–3658, doi:10.5194/acp-17-3637-2017, 2017.

Vergara-Temprado, J., Miltenberger, A. K., Furtado, K., Grosvenor, D. P., Shipway, B. J., Hill, A. A., Wilkinson, J. M., Field, P. R., Murray, B. J. and Carslaw, K. S.: Strong control of Southern Ocean cloud reflectivity by ice-nucleating particles, Proc. Natl. Acad. Sci., 115(11), 201721627, doi:10.1073/pnas.1721627115, 2018.

Villa, T., Salimi, F., Morton, K., Morawska, L. and Gonzalez, F.: Development and Validation of a UAV Based System for Air Pollution Measurements, Sensors, 16(12), 2202, doi:10.3390/s16122202, 2016.

Wang, B., Harder, T. H., Kelly, S. T., Piens, D. S., China, S., Kovarik, L., Keiluweit, M., Arey, B. W., Gilles, M. K. and Laskin, A.: Airborne soil organic particles generated by precipitation, Nat. Geosci., 9(6), 433–437, doi:10.1038/ngeo2705, 2016.

Von Der Weiden, S.-L., Drewnick, F. and Borrmann, S.: Particle Loss Calculator – a new software tool for the assessment of the performance of aerosol inlet systems, Atmos. Meas. Tech, 2, 479–494 [online] Available from: www.atmos-meas-tech.net/2/479/2009/ (Accessed 12 January 2018), 2009.

Welti, A., Lüönd, F., Stetzer, O. and Lohmann, U.: Influence of particle size on the ice nucleating ability of mineral dusts, Atmos. Chem. Phys., 9(18), 6705–6715, doi:10.5194/acp-9-6705-2009, 2009.

Wex, H., Huang, L., Zhang, W., Hung, H., Traversi, R., Becagli, S., Sheesley, R. J., Moffett, C. E., Barrett, T. E., Bossi, R., Skov, H., Hünerbein, A., Lubitz, J., Löffler, M., Linke, O., Hartmann, M., Herenz, P. and Stratmann, F.: Annual variability of ice-nucleating particle concentrations at different Arctic locations, Atmos. Chem. Phys., 19(7), 5293–5311, doi:10.5194/acp-19-5293-2019, 2019.

Whale, T. F., Murray, B. J., O'Sullivan, D., Wilson, T. W., Umo, N. S., Baustian, K. J., Atkinson, J. D., Workneh, D. A. and Morris, G. J.: A technique for quantifying heterogeneous ice nucleation in microlitre supercooled water droplets, Atmos. Meas. Tech., 8(6), 2437–2447, doi:10.5194/amt-8-2437-2015, 2015.

741   Zhao, B., Wang, Y., Gu, Y., Liou, K.-N., Jiang, J. H., Fan, J., Liu, X., Huang, L. and Yung, Y. L.: Ice nucleation

742   by aerosols from anthropogenic pollution, Nat. Geosci., 12(8), 602–607, doi:10.1038/s41561-019-0389-4, 2019.

743

744
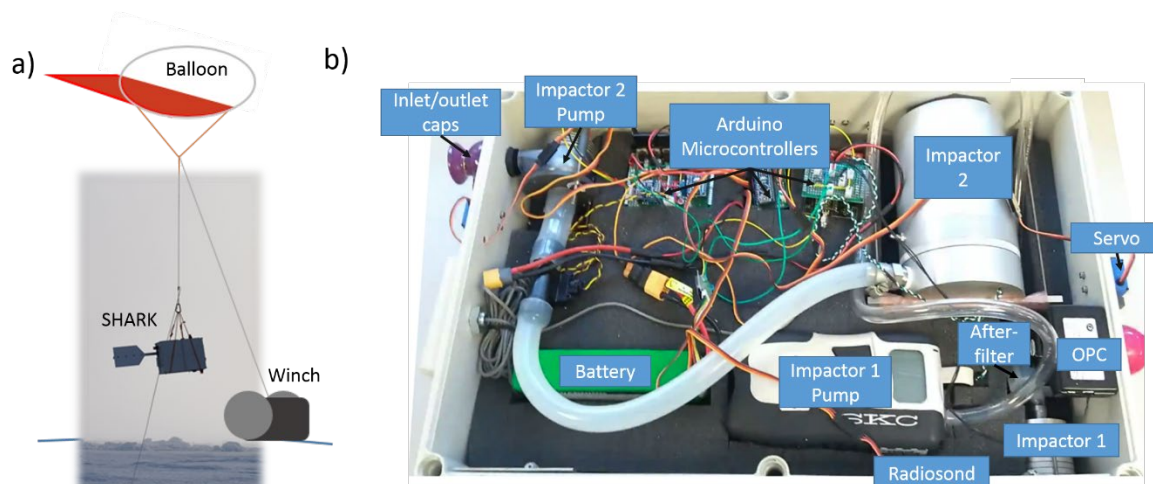
Figure 1. The SHARK. (a) The SHARK payload on a tethered balloon connected to ground by a winch. The photograph was taken during deployment in the High Arctic. (b) The components inside the SHARK payload labelled on a photograph. The payload featured a large impactor inlet at the top of the platform for Impactor 2, with the OPC inlet facing the front, and a small impactor inlet at the bottom for Impactor 1. The radiosond was at the bottom of the box, and the outlet valve for the pump system is shown at the back of the SHARK, where the 100 L min^{-1} pump for Impactor 2 vents.
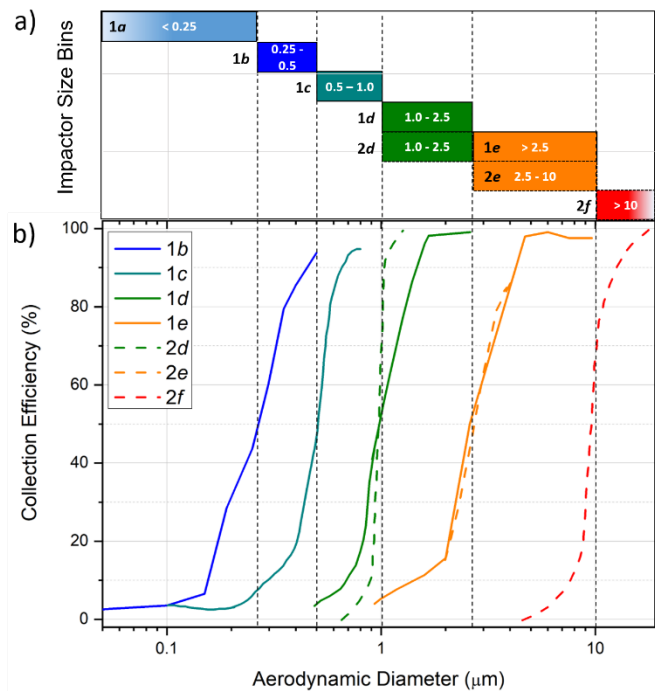
Figure 2. Collection efficiencies of each size bin of the two cascade impactors in the SHARK. (a) The size bins for each stage of Impactor 1 and 2 at flow rates of 9 and 100 L min^{-1}, respectively. (b) Impactor efficiency curves for each stage. Impactor 1 has four stages (1*b-e*) and one after-filter (1*a*), while Impactor 2 has three stages (2*d-f*). Stages 1*d* and 2*d* as well as 1*e* and 2*e* should be approximately equivalent in terms of the aerosol size ranges collected.
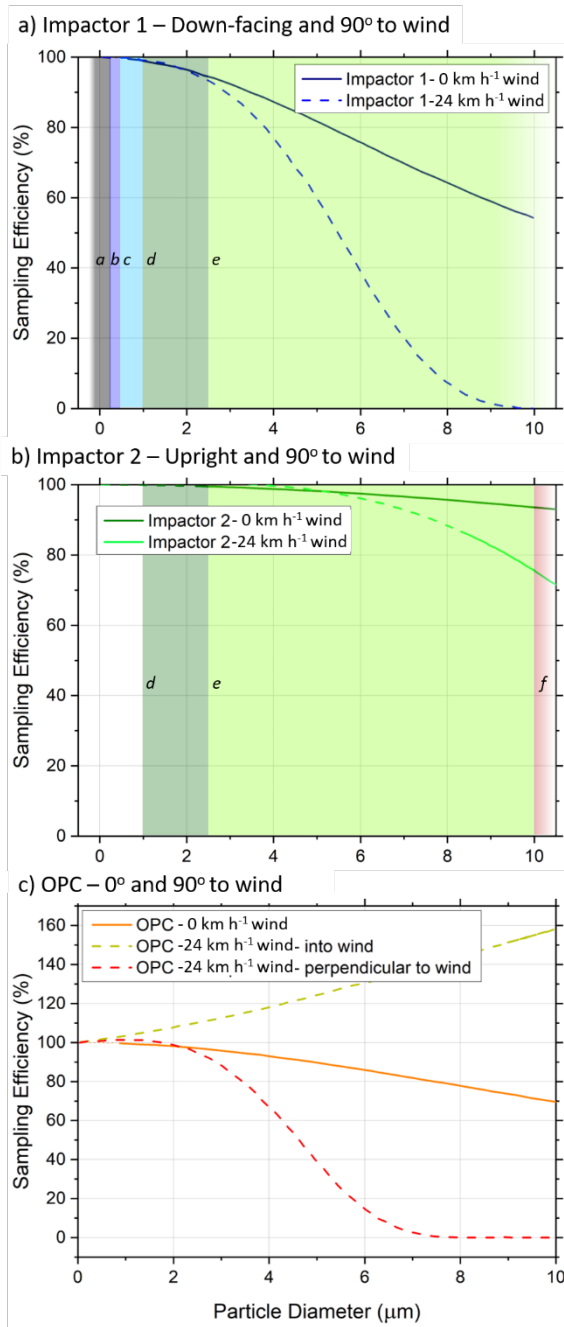
Figure 3. SHARK sampling efficiencies (a) The sampling efficiencies of Impactor 1, with and without wind, when sampling at 90° to the wind direction. (b) The sampling efficiencies of Impactor 2, with and without wind, when sampling at 90° to the wind direction. (c) The sampling efficiency of the OPC, with and without wind, when sampling at 0° and 90° to the wind direction (the OPC was deployed at 0° to the wind, based on this calculation). Solid lines denote model predictions within the formulas' validity range, and dotted lines represent approximations (Von Der Weiden et al., 2009).
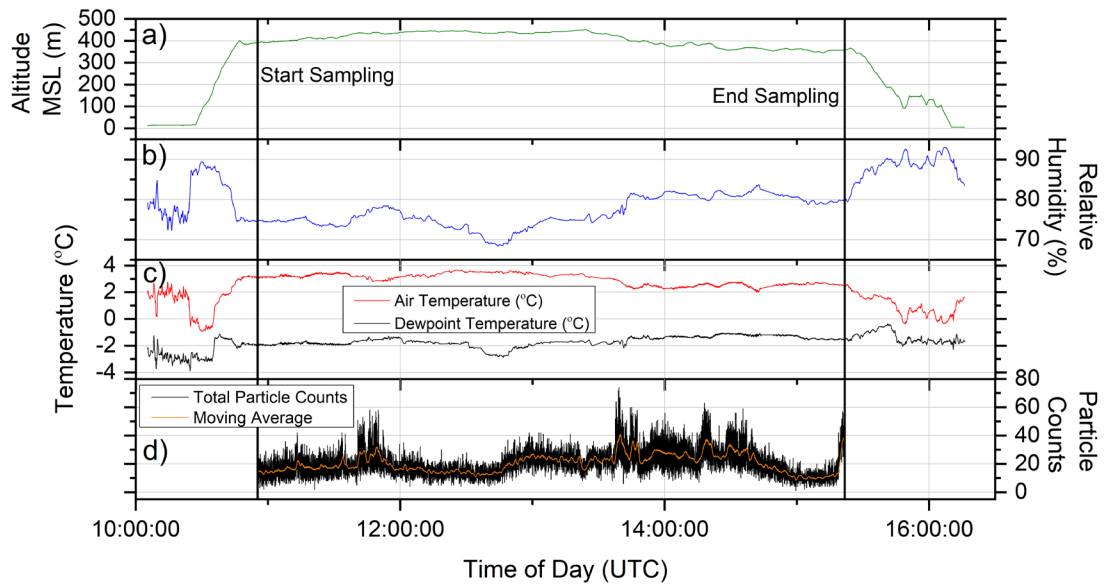
Figure 4. Windsond and optical particle counter (OPC) data for a flight during a campaign to the High Arctic. (a) The altitude of the SHARK payload throughout the 4.5 hour flight. The sampling start and end times are indicated as solid lines. The SHARK reached 450 above Mean Sea Level (MSL) and in the last hour of flight was lowered to 350 m due to ice formation on the balloon, instrument and tether. (b) The humidity during the flight was monitored to ensure the SHARK was not sampling during unfavourable conditions. The SHARK was brought back down to ground level once the sampling had been stopped. (c) The ambient temperature was monitored alongside the dewpoint temperature. (d) Total particle counts throughout the sampling period, as monitored by the OPC.
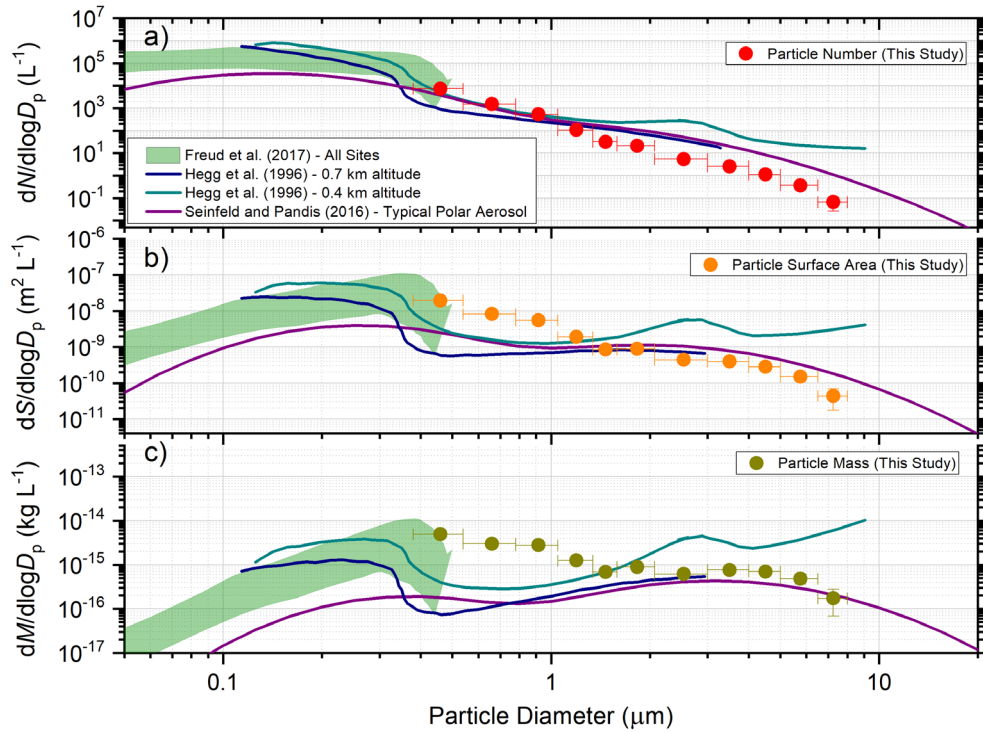
Figure 5. Size distribution data produced from OPC measurements. (a) Particle number, (b) particle surface area and (c) particle mass size distribution data above the surface temperature inversion during a test run of the SHARK suite whilst deployed on a tethered balloon in the High Arctic. Comparisons to previous studies at Arctic sites are shown (Freud et al., 2017; Hegg et al., 1996; Seinfeld and Pandis, 2016). The August aerosol number size distributions for all listed sites in Freud et al., including Zeppelin, Nord, Alert, Barrow and Tiksi are shown. The data from Hegg et al., at altitudes of 0.7 km and 0.4 km in Prudhoe Bay, Alaska, are presented. The size distributions from Seinfeld and Pandis are calculated given the parameters for multimode distributions given in Table 8.3.
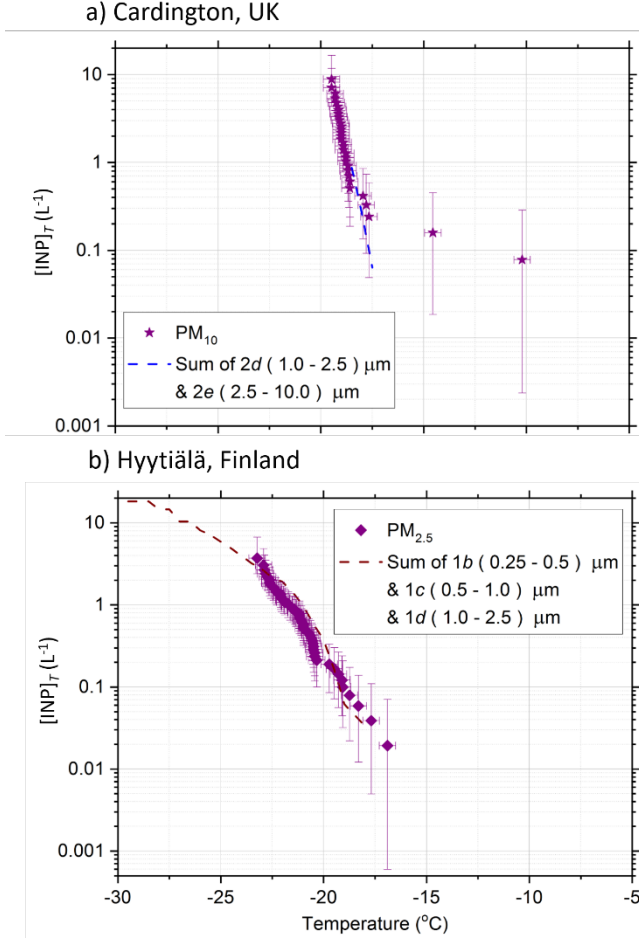
Figure 6. The sum of INP concentrations, $[INP]_T$, for labelled stages measured at: (a) Cardington (UK) and (b) Hyytiälä (Finland) alongside data from a standard sampler. Cardington data was taken from Impactor 2 whilst on a tethered balloon at 20 m above ground level, and is shown against a PM_{10} sampler at ground level. Hyytiälä data was collected using Impactor 1 at ground level, alongside a $PM_{2.5}$ sampler. The dotted lines indicate the sum of the INP concentrations for the SHARK impactor stages, calculated by weighting $f_{ice}(T)$ to the volume of sampled air, and summing the concentrations in each temperature bin.
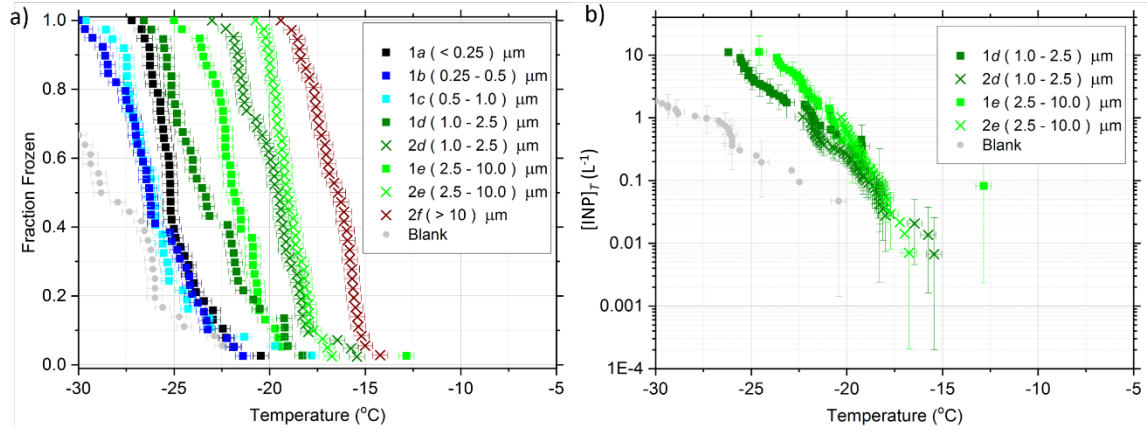
Figure 7. Ice-nucleating particle (INP) analysis of samples collected in Leeds (UK) using the SHARK. (a) The fraction of droplets frozen as a function of temperature, $f_{ice}(T)$, for each stage of Impactors 1 and 2. The handling blank is shown in grey. (b) The INP concentrations for stage 'e' of both impactors (2.5-10 μm), highlighting their excellent agreement.
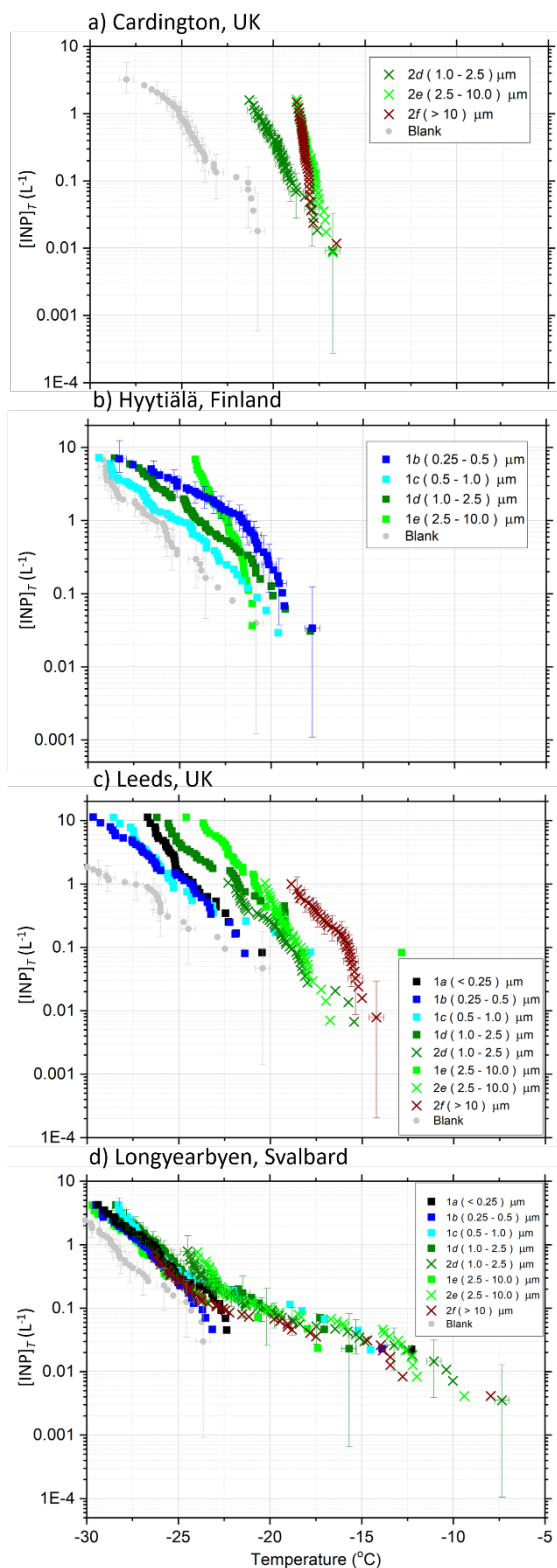
Figure 8. INP concentrations determined from each impactor stage of the SHARK at the four testing sites: (a) Cardington (UK), (b) Hyytiälä (Finland), (c) Leeds (UK) and (d) Longyearbyen (Svalbard). Handling blank data, which determine the baseline of the results, are shown in grey. Samples of the error bars are shown.
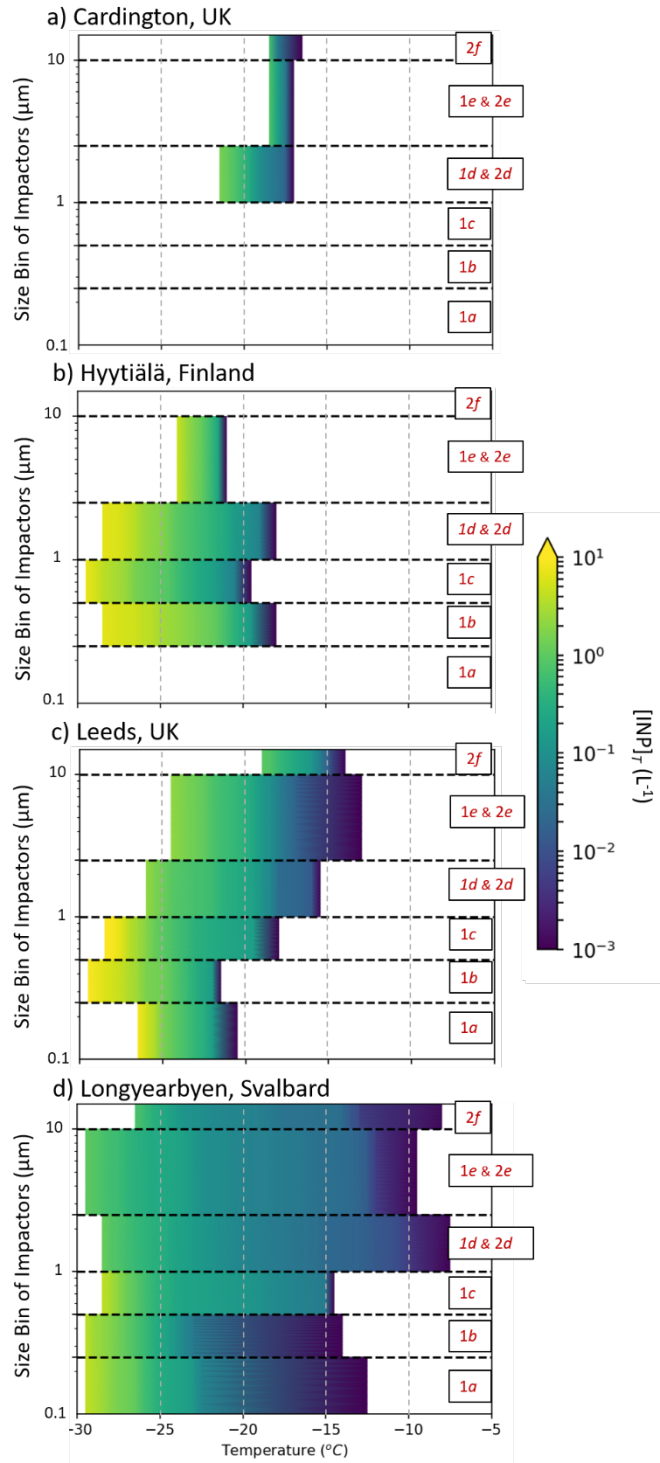
Figure 9. Size-resolved ice-nucleating particle concentrations (sr[INP]$_T$) for the four test sites: (a) Cardington (UK), (b) Hyytiälä (Finland), (c) Leeds (UK) and (d) Longyearbyen (Svalbard). The colour bars indicate the INP concentration. The dotted lines on the y-axis indicate the size cuts of the impactors. The data from Figure 8 is presented here in an alternative format, which has the advantage of more clearly and concisely displaying the features of the INP spectrum in each size bin than the plots in Fig 8.
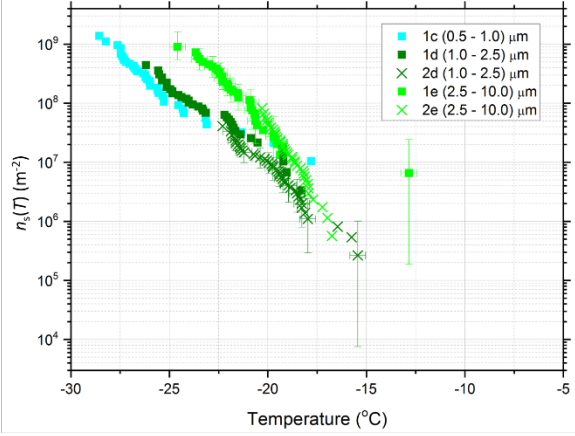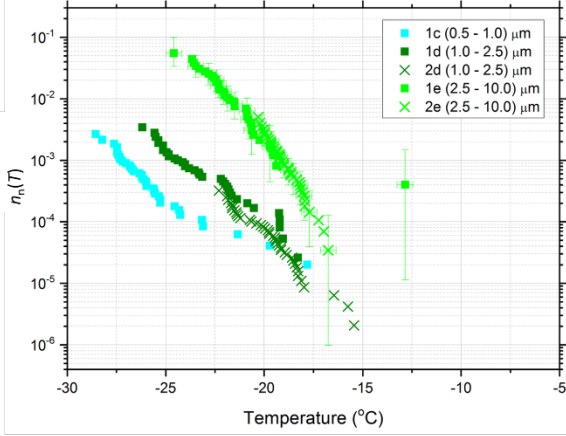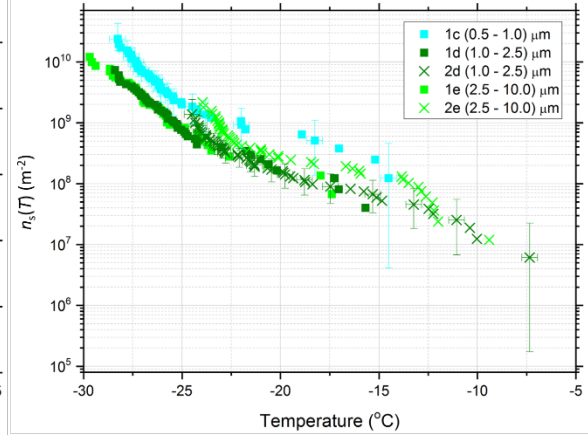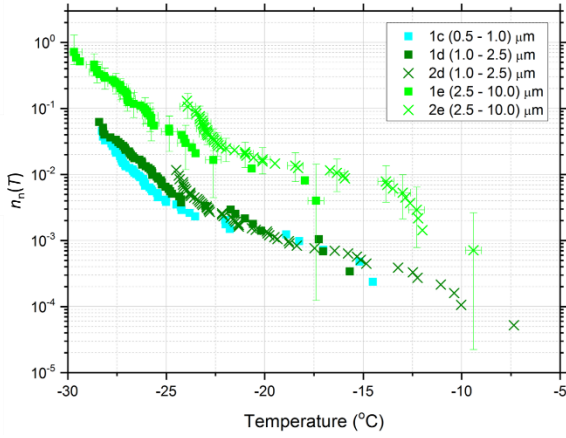
Figure 10. Plots showing (left) the activated fraction of aerosol ($n_n(T)$) and (right) the number of active sites per surface area ($n_s(T)$) for samples tested from two measurement sites: (a) Leeds (UK) and (b) Longyearbyen (Svalbard). The colours of the data points indicate the size bins of each impactor, and the different symbols represent the two impactors. Samples of the error bars are shown.